

NAVAL POSTGRADUATE SCHOOL Monterey, California



THESIS

MODELING THE BIODYNAMICAL RESPONSE OF THE
HUMAN HEAD FOR INJURY ANALYSIS

by

Danielle N. George

September 2001

Thesis Advisor:

Young W. Kwon

Approved for public release; distribution is unlimited.

Report Documentation Page

Report Date 30 Sep 2001	Report Type N/A	Dates Covered (from... to) -
Title and Subtitle Modeling the Biodynamical Response of the Human Head for Injury Analysis	Contract Number	
	Grant Number	
	Program Element Number	
Author(s) George, Danielle N.	Project Number	
	Task Number	
	Work Unit Number	
Performing Organization Name(s) and Address(es) Research Office Naval Postgraduate School Monterey, Ca 93943-5138	Performing Organization Report Number	
Sponsoring/Monitoring Agency Name(s) and Address(es)	Sponsor/Monitor's Acronym(s)	
	Sponsor/Monitor's Report Number(s)	
Distribution/Availability Statement Approved for public release, distribution unlimited		
Supplementary Notes		
Abstract		
Subject Terms		
Report Classification unclassified	Classification of this page unclassified	
Classification of Abstract unclassified	Limitation of Abstract UU	
Number of Pages 107		

REPORT DOCUMENTATION PAGE			Form Approved OMB No. 0704-0188	
Public reporting burden for this collection of information is estimated to average 1 hour per response, including the time for reviewing instruction, searching existing data sources, gathering and maintaining the data needed, and completing and reviewing the collection of information. Send comments regarding this burden estimate or any other aspect of this collection of information, including suggestions for reducing this burden, to Washington headquarters Services, Directorate for Information Operations and Reports, 1215 Jefferson Davis Highway, Suite 1204, Arlington, VA 22202-4302, and to the Office of Management and Budget, Paperwork Reduction Project (0704-0188) Washington DC 20503.				
1. AGENCY USE ONLY (Leave blank)		2. REPORT DATE September 2001		3. REPORT TYPE AND DATES COVERED Master's Thesis
4. TITLE AND SUBTITLE Modeling the Biodynamical Response of the Human Head for Injury Analysis				5. FUNDING NUMBERS
6. AUTHOR (S) George, Danielle N.				
7. PERFORMING ORGANIZATION NAME(S) AND ADDRESS(ES) Naval Postgraduate School Monterey, CA 93943-5000				8. PERFORMING ORGANIZATION REPORT NUMBER
9. SPONSORING / MONITORING AGENCY NAME(S) AND ADDRESS(ES)				10. SPONSORING/MONITORING AGENCY REPORT NUMBER
11. SUPPLEMENTARY NOTES The views expressed in this thesis are those of the author and do not reflect the official policy or position of the U.S. Department of Defense or the U.S. Government.				
12a. DISTRIBUTION / AVAILABILITY STATEMENT Approved for public release; distribution is unlimited				12b. DISTRIBUTION CODE A
13. ABSTRACT (maximum 200 words) The objective of this study is to develop a finite element model of the human head and neck to investigate the biomechanics of head injury. The finite element model is a two-dimensional, plane strain representation of the cervical spine, skull, and major components of the brain including the cerebrum, cerebellum, brain stem, tentorium and the surrounding cerebral spinal fluid. The dynamic response of the model is validated by comparison with the results of human volunteer sled acceleration experiments conducted by Ewing et al. [10]. To validate the head model, one of the head impact experiments performed on cadavers by Nahum et al. [24], is simulated. The model responses are compared with the measured cadaveric test data in terms of head acceleration, and intracranial pressures measured at four locations including the coup and contrecoup sites. The validated model is used to demonstrate that the Head Injury Criterion (HIC), which is based on resultant translational acceleration of the center of gravity of the head, does not relate to the various mechanisms of brain injury and is therefore insufficient in predicting brain injury.				
14. SUBJECT TERMS Finite Element Modeling, Human Head Model, Impact Analysis, Brain Injury				15. NUMBER OF PAGES
				16. PRICE CODE
17. SECURITY CLASSIFICATION OF REPORT Unclassified		18. SECURITY CLASSIFICATION OF THIS PAGE Unclassified		19. SECURITY CLASSIFICATION OF ABSTRACT Unclassified
				20. LIMITATION OF ABSTRACT UL

NSN 7540-01-280-5500

Standard Form 298 (Rev. 2-89)
Prescribed by ANSI Std. Z39-18

THIS PAGE INTENTIONALLY LEFT BLANK

Approved for public release; distribution is unlimited

**MODELING THE BIODYNAMICAL RESPONSE OF THE HUMAN HEAD FOR
INJURY ANALYSIS**

Danielle N. George
Lieutenant, United States Navy
B.S.M.E., San Jose State University, 1994

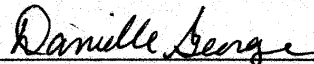
Submitted in partial fulfillment of the
requirements for the degree of

MASTER OF SCIENCE IN MECHANICAL ENGINEERING

from the

**NAVAL POSTGRADUATE SCHOOL
September 2001**

Author:

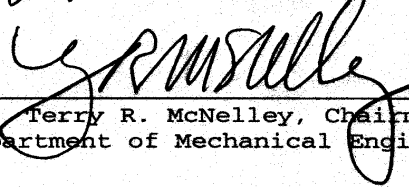


Danielle N. George

Approved by:



Young W. Kwon, Thesis Advisor



Terry R. McNelley, Chairman
Department of Mechanical Engineering

THIS PAGE INTENTIONALLY LEFT BLANK

ABSTRACT

The objective of this study is to develop a finite element model of the human head and neck to investigate the biomechanics of head injury. The finite element model is a two-dimensional, plane strain representation of the cervical spine, skull, and major components of the brain including the cerebrum, cerebellum, brain stem, tentorium and the surrounding cerebral spinal fluid. The dynamic response of the model is validated by comparison with the results of human volunteer sled acceleration experiments conducted by Ewing et al. [10]. To validate the head model, one of the head impact experiments performed on cadavers by Nahum et al. [24], is simulated. The model responses are compared with the measured cadaveric test data in terms of head acceleration, and intracranial pressures measured at four locations including the coup and contrecoup sites. The validated model is used to demonstrate that the Head Injury Criterion (HIC), which is based on resultant translational acceleration of the center of gravity of the head, does not relate to the various mechanisms of brain injury and is therefore insufficient in predicting brain injury.

THIS PAGE INTENTIONALLY LEFT BLANK

TABLE OF CONTENTS

I.	INTRODUCTION	1
II.	BACKGROUND	5
A.	HUMAN ANATOMY	5
1.	The Spine	5
2.	The Head	12
a.	<i>The Scalp</i>	12
b.	<i>The Skull</i>	13
e.	<i>The Meninges</i>	17
d.	<i>The Brain</i>	18
B.	LITERATURE REVIEW	23
III.	HEAD INJURY	35
A.	TYPES AND BIOMECHANICAL MECHANISMS OF HEAD INJURY	35
1.	Diffuse Injury	36
2.	Focal Injury	39
B.	HEAD INJURY CRITERIA	41
C.	OTHER PROPOSED INJURY TOLERANCE CRITERIA	44
V.	FINITE ELEMENT MODEL	47
A.	SPINE	47
B.	HEAD	48
V.	RESULTS AND DISCUSSION	53
A.	MODEL VALIDATION	53
1.	Ewing Sled Test	53
a.	<i>Method and Simulation</i>	53
b.	<i>Results</i>	54
2.	Nahum Cadaver Head Impact Tests	58
a.	<i>Method and Simulation</i>	58
b.	<i>Results</i>	60
B.	PARAMETRIC STUDY	66
1.	Effects of impact force characteristics	68
2.	Effects of impactor characteristics	76
VI.	CONCLUSIONS AND RECOMMENDATIONS	83
A.	CONCLUSIONS	83
B.	RECOMMENDATIONS	85
	LIST OF REFERENCES	87
	INITIAL DISTRIBUTION LIST	91

THIS PAGE INTENTIONALLY LEFT BLANK

LIST OF FIGURES

Figure 1.	Lateral (left) and Frontal (right) Views of the Human Spine. From Ref. [3].	6
Figure 3.	Occiput-Atlas-Axis Articulation. The Attachment of the Alar Ligaments to the Dens and to the Occipital Condyle is Shown. After Ref. [37].	9
Figure 4.	First Cervical Vertebra, or Atlas. From Ref. [13].	9
Figure 5.	Second Cervical Vertebra, or Axis. From Ref. [13].	10
Figure 6.	Intervertebral Disk Sectioned to Expose the Annular Organization. From Ref. [3].	11
Figure 7.	Ligaments of the Spine. From Ref. [37].	12
Figure 8.	Side View of the Human Skull. From Ref. [2].	14
Figure 9.	The Human Skull: (a) Inferior and (b) Superior View, with Cranium Removed. From Ref. [2].	16
Figure 10.	Structures Enclosing the Nervous System. (a) Relationship of the Brain and Spinal Cord to the Bones that Enclose them. (b) Details of the Three Layers of the Meninges. From Ref. [2].	18
Figure 11.	The Human Brain in Position in the Skull as Seen from the Lateral Aspect. From Ref. [2].	19
Figure 12.	Injury Risk Curve for HIC. From Ref. [18].	43
Figure 13.	Finite Element Model of the Head and Neck.	52
Figure 14.	Finite Element Model Simulating Sled Acceleration Test.	54
Figure 15.	Vertical Displacement of the Head	55
Figure 16.	Head CG X-Acceleration	57
Figure 17.	Head CG Y-Acceleration	57
Figure 18.	Frontal Impact Model Configuration.	59
Figure 19.	Impact Force	60
Figure 20.	Head Acceleration	61
Figure 21.	Frontal Hydrostatic Stress (Pressure)	62
Figure 22.	Posterior Fossa Hydrostatic Stress (Pressure)	63
Figure 23.	Occipital Hydrostatic Stress (Pressure)	64
Figure 24.	Parietal Hydrostatic Stress (Pressure)	65
Figure 25.	Hydrostatic Stress (Pressure) Contours at 3 ms	66
Figure 26.	Force Profiles Used in Parametric Study.	67
Figure 27.	Head CG Acceleration by Location.	69
Figure 28.	Pressure by Location.	70
Figure 29.	Pressure Versus Acceleration for Frontal Impact.	71
Figure 30.	Pressure Versus Acceleration for Occipital Impact.	71

Figure 31.	Pressure Versus Acceleration for Crown Impact...	72
Figure 32.	HIC by Location.....	73
Figure 33.	Normalized Parameters Versus Acceleration for Frontal Impact.....	74
Figure 34.	Normalized Parameters Versus Acceleration for Occipital Impact.....	75
Figure 35.	Normalized Parameters Versus Acceleration for Crown Impact.....	75
Figure 36.	Head CG Acceleration by Location.....	77
Figure 37.	Pressure by Location.....	78
Figure 38.	Pressure Versus Acceleration for Frontal Impact.....	78
Figure 39.	Pressure Versus Acceleration for Occipital Impact.....	79
Figure 40.	Pressure Versus Acceleration for Crown Impact...	79
Figure 41.	Acceleration Versus Momentum for Frontal, Occipital and Crown Impacts.....	80
Figure 42.	Pressure Versus Momentum for Frontal, Occipital and Crown Impacts.....	81
Figure 43.	Acceleration Versus Kinetic Energy for Frontal, Occipital and Crown Impacts.....	82
Figure 44.	Pressure Versus Kinetic Energy for Frontal, Occipital and Crown Impacts.....	82

LIST OF TABLES

Table 1.	Abbreviated Injury Scale Severity Codes. From Ref. [18].	42
Table 2.	Material Properties of the Cervical Spine Used in Model.	48
Table 3.	Various Material Properties of the Head from the Literature.	50
Table 4.	Material Properties of the Head Used in Model.	51

THIS PAGE INTENTIONALLY LEFT BLANK

ACKNOWLEDGEMENTS

I would like to thank Professor Young W. Kwon for his support throughout this research. His guidance has significantly enhanced my education at the Naval Postgraduate School. I would also like to thank Professor Josh Gordis for his assistance in learning the Patran/Nastran finite element analysis program and Jim Mahoney for his time and assistance in overcoming computer hardware limitations and software problems. Finally, I would like to thank my parents, family and friends for their moral support, patience and understanding which significantly contributed to the motivation in completing this thesis research.

THIS PAGE INTENTIONALLY LEFT BLANK

I. INTRODUCTION

Head injury is a traumatic insult to the brain. Although not always visible, it may cause enduring physical, emotional, intellectual and social changes for the survivor. The impact of the head injury goes beyond the survivor. Long term effects place an enormous emotional and financial burden on the individual's family, and strain medical and other service systems due to the high costs and often life-long needs [11].

Some of the head injury statistics are truly astounding. According to a recent report compiled by the National Institute of Health, in the United States alone, it is estimated that there are over two million traumatic brain injuries per year, with 500,000-750,000 severe enough to require hospitalization while 75,000-100,000 result in death [25]. To get an idea of the magnitude of the problem, consider that over the past 12 years, death from head injury has exceeded the cumulative number of American battle deaths inclusive of all wars since the founding of the Republic [25]. Overall, head injuries represent 2% of all deaths, and 26% of all injury deaths [11]. Among survivors, many will suffer long-term disabilities or permanent neurological deficits even from head injury cases, that are considered mild [11].

It is no surprise that motor vehicle crashes are the leading cause of traumatic brain injuries, accounting for 51%. Falls are the second leading cause, at 21%; followed by assaults and violence 12%; and sports and recreation 10% [11,25]. It is also interesting to note that a person does

not have to be "knocked out" or even strike their head in order to sustain a traumatic brain injury (TBI), for example, whiplash injuries can result in TBI [25].

The costs of head injury are staggering. Nationwide, the total economic costs for all head injuries approach \$25 billion per year in direct and indirect costs of medical, rehabilitative and support services, and lost wages. For an individual, the lifetime costs for care of a head injury survivor are estimated to be between \$4.1 million and \$9 million.

Adequate protection of the head is critical since anatomic injuries to the structures of the brain are currently nonreversible and the consequences of injury can be devastating [22]. But brain injury and the mechanisms, which cause injury, are complex and not completely understood. Head injury mechanisms are difficult to study experimentally due to the variety of impact conditions involved as well as ethical issues, such as the use of human cadavers and animals [17]. The data from experiments conducted on animals and cadavers is further limited to the specific test conducted and by variation in physical and material properties of the test subjects.

Numerous mathematical models have been developed and analyzed over the past 30 years in an effort to gain a better understanding of brain injury mechanisms. Of these models, finite element modeling seems to be the best method for brain injury analysis because of its capability of handling complex geometries, and different kinds of nonlinearities of geometrical and physical nature. Furthermore, finite element models can provide field

distribution measures such as stress, strain and pressure that, when used in conjunction with experimental data, can be correlated to injury mechanisms [7,32].

A finite element model must first be validated to have any relevance to the biomechanical response of the brain. Experimental modeling of head impact is essential in the model validation process by providing measured force, acceleration and displacement data from experiments for direct comparison with model response.

A validated human head model can become a powerful tool to correlate mechanical parameters involved in brain injury to clinical observations and to investigate the injury mechanisms due to various inputs [14]. In addition to allowing the assessment of different experimental impact conditions, finite element models can be used to predict the response to injury producing conditions that cannot be simulated experimentally, and they can predict responses that cannot be measured in animal and cadaver experiments. Models are means by which valid experimental animal and cadaveric data can be extrapolated to living man [17]. Then by relating the various mechanical parameters of model response to injury, tolerance criteria can be formulated.

The objective of this study is to develop a finite element model of the human head and neck such that the model adequately represents the biodynamical response to direct head impact and inertial loading. The model is used to investigate the biomechanics of head injury and injury mechanisms. The dynamic response of the head-neck model is validated by comparison with the results of human volunteer sled acceleration experiments. Validation of the head

model is accomplished by comparing the model's response with measured cadaveric impact test data. Once the model is validated, a parametric study is conducted to determine the effects of different impact force characteristics and impact location.

II. BACKGROUND

A brief summary of the key anatomical components of the human head-neck complex will be given to provide a basic description and rationale for the finite element modeling of the head and neck. Although the cervical spine is of primary importance for this study, the entire spine is modeled in order to facilitate the simulation of the sled acceleration test used for model validation.

A. HUMAN ANATOMY

1. The Spine

The muscles and other soft tissue of the neck are not included in the finite element model for this study and therefore will not be discussed in detail. As mentioned above, the primary focus of the neck model is on the cervical spine. A discussion of the common components of the entire spine and more specific details of the cervical spine will be addressed.

The function of the spine is to form a strong support structure for the head and trunk, to protect the spinal cord, and to provide rigidity for the suspension of limbs. The spine is divided into four primary regions: cervical, thoracic, lumbar and sacral as shown in Figure 1. Together, these regions consist of 24 presacral vertebra that are separated by relatively flexible intervertebral disks and 5 sacral vertebrae, which are fused. The vertebrae and disks along with seven intervertebral ligaments spanning each set of adjacent vertebrae, and two synovial joints on each vertebra called the facet joints, act to constrain relative motion. The vertebrae of each spinal section are numbered starting with the uppermost

vertebra. For example, the first cervical vertebra is denoted C1 and the lowermost cervical vertebra is C7 and the first thoracic vertebra is T1 and so on [5,20].

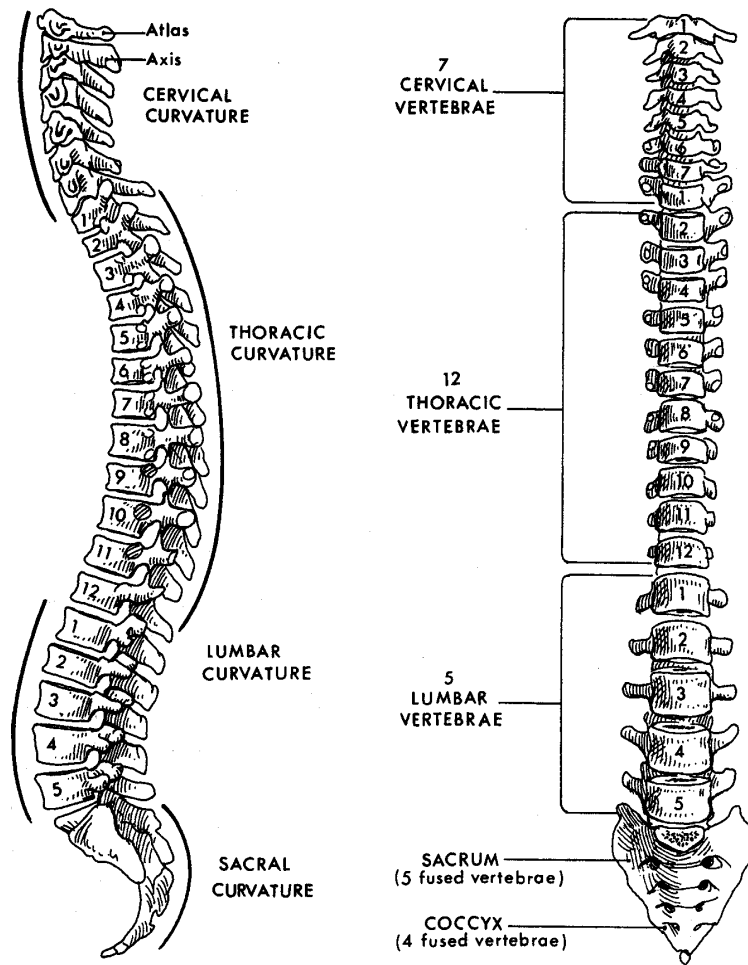


Figure 1. Lateral (left) and Frontal (right) Views of the Human Spine. From Ref. [3].

With the exception of the upper cervical vertebrae, C1 and C2 (also known as the atlas and axis), each vertebra is geometrically similar but increasing in size from superior to inferior. Each of these vertebra are composed of a

cylindrical vertebral body connected to a complex configuration of posterior and lateral structures. A motion segment of the lumbar spine is shown as an example in Figure 2. This configuration includes the pedicles and laminae that form the neural arch which completes the spinal canal providing mechanical protection for the spinal cord and contributing to the stability of the vertebral column. Also part of this configuration are the spinous and transverse processes, which serve primarily as muscle attachment sites. The transverse process also contains the vertebral artery, which is the major blood supply for the brainstem and the posterior portions of the brain. Additionally, each vertebra has right and left superior and inferior articular processes forming the right and left facet joints. These are synovial joints, which are wrapped in a capsular ligament. The main role of the facet joints is to limit the excessive intervertebral shear and torsion motions of the intervertebral segment. This effect is particularly pronounced in the cervical spine, where the facet joints cause marked coupling between lateral bending and axial torsion motions [20].

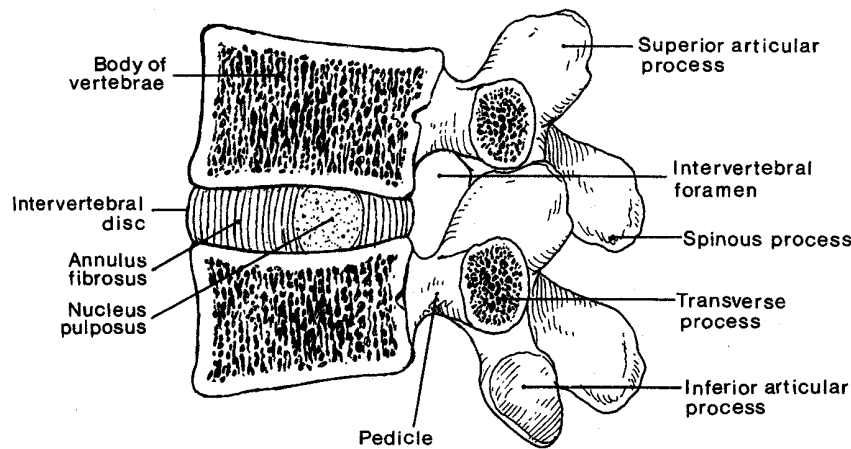


Figure 2. Lumbar Spine Motion Segment. Medial View of Right Half when Sectioned in the Midsagittal Plane. Ligaments are Omitted for Clarity. From Ref. [3].

The upper cervical spine is composed of the C1 and C2 vertebrae (atlas and axis) and the base of the skull, called the occiput. The occipitoatlantal joint is formed by the occipital condyles, which are bony protuberances on the base of the skull, and the atlas. The atlantoaxial joint is composed of the three synovial articulations between the atlas and axis as shown in Figure 3.

The structures of the atlas and axis differ from that of the other vertebrae in order to facilitate a relatively wide range of motion of the head. The atlas, which supports the skull, is a ring shaped bone, with large facet joints on the lateral portions and no vertebral body as illustrated in Figure 4.

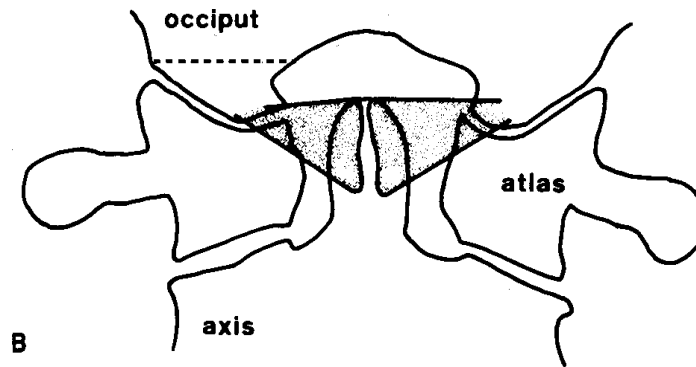


Figure 3. Occiput-Atlas-Axis Articulation. The Attachment of the Alar Ligaments to the Dens and to the Occipital Condyle is Shown. After Ref. [37].

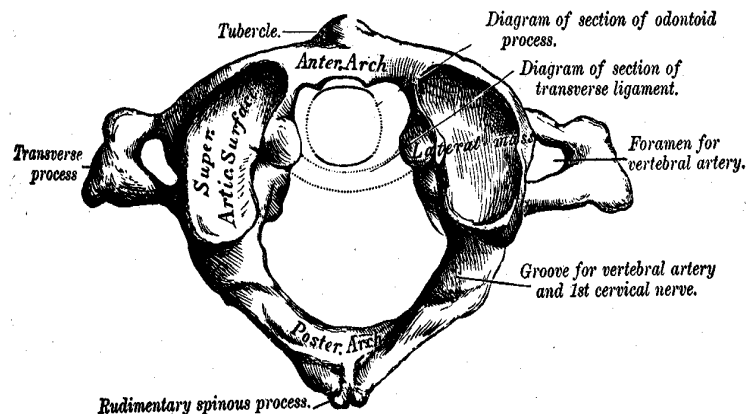


Figure 4. First Cervical Vertebra, or Atlas. From Ref. [13].

The axis is composed of a vertebral body, a posterior bony arch and an additional structure called the odontoid process or dens [20]. The dens is elongated vertically and forms a longitudinal axis about which the atlas and the occiput rotate. The lateral portions of the axis contain

enlarged articular facet surfaces. The axis is illustrated in Figure 5.

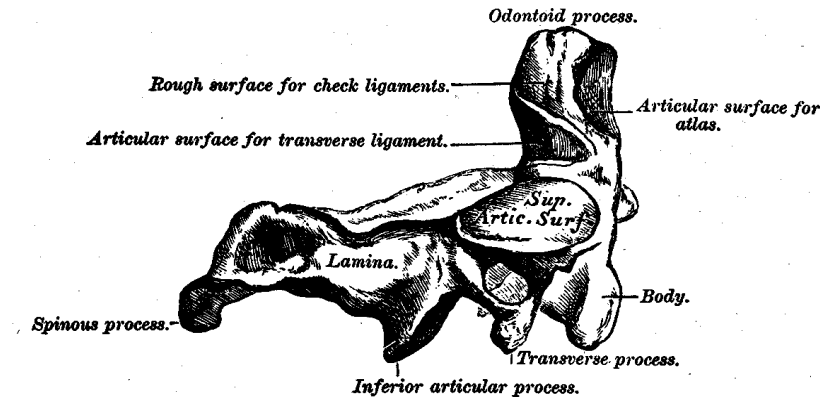


Figure 5. Second Cervical Vertebra, or Axis. From Ref. [13].

The motion around this axis is constrained by the strong transverse and odontoid ligaments and the Occ-C1 and C1-2 facet joints [3].

The vertebral body consists of trabecular bone surrounded by a thin cortical shell. The trabecular bone provides resistance to compression and shear loading. A fibrocartilaginous joint, the intervertebral disk, connects by means of the articular process and the vertebral bodies. The intervertebral disk, acts as a flexible spacer between adjacent vertebrae and carries significant compressive loads. The disk behaves as a thick-walled deformable annulus that, until degenerate, contains fluid under pressure [3].

The disk is composed of the inner fluid-like nucleus pulposus bounded by a laminar set of spirally wound fibrous sheets of the outer annulus fibrosis as shown in Figure 6.

When an axial load is applied to the disk, the external force is resisted by several mechanisms, including an elevated nucleus pressure. The material of the nucleus develops an osmotic swelling pressure which balances the applied stress. If the applied stress is increased water is driven out of the disk or if the applied stress is reduced the disk rehydrates to maintain equilibrium [3,20].

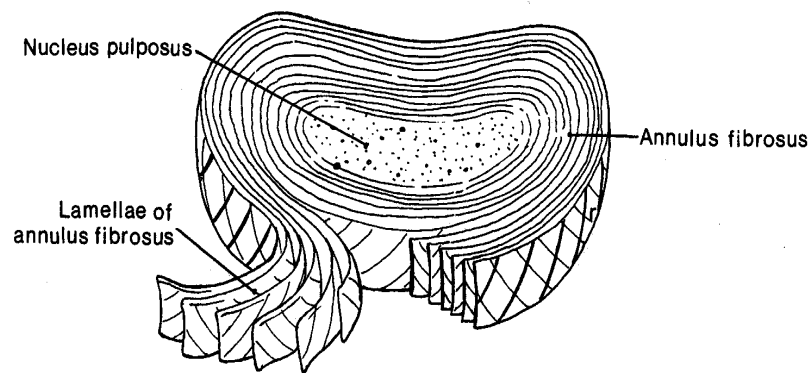


Figure 6. Intervertebral Disk Sectioned to Expose the Annular Organization. From Ref. [3].

The ligaments of the spine can be divided into five sets. There are those connecting the bodies of the vertebrae, the laminae, the articular processes, the spinous processes, and those connecting the transverse processes. The most important are the interspinous and supraspinous ligaments. The interspinous ligament is thin and membranous and extends from the root of the summit of the spinous process between each vertebra. The supraspinous ligament is a strong cord connecting the

spinous processes from the seventh cervical vertebra to the sacrum. The flaval, yellow, ligaments similarly connect adjacent lamina from the sacrum to the base of the skull [13,20]. Figure 7. depicts the major ligaments.

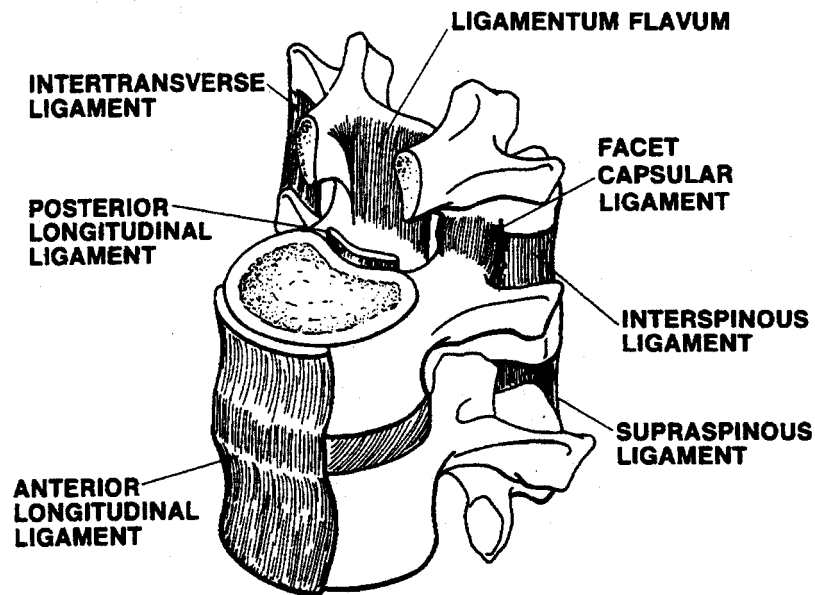


Figure 7. Ligaments of the Spine. From Ref. [37].

2. The Head

a. The Scalp

The scalp is 5 to 7 mm (0.20 to 0.28 inches) thick and consists of three layers: the cutaneous outer layer, a subcutaneous connective tissue layer, and a muscle a facial layer. Beneath the scalp there is a loose connective tissue layer and the periosteum which is a fibrous membrane covering the bone [22].

b. The Skull

The human skull is a complex structure of irregular shaped bones, which, with the exception of the lower jaw, are fused at the sutures. It is divided into two parts: the cranium and the face. There are 22 bones in all, with 8 belonging to the cranium and 14 to the face [fig skull side view]. The thickness of the skull varies between 4 and 7 mm (0.16 and 0.28 in) and consists of three layers; a spongy diploe layer sandwiched between dense inner and outer layers. The primary purpose of the cranium is to house and protect the brain. Therefore the cranium and its internal surfaces will be of primary concern for this study. The eight cranial bones include the occipital bone, two parietal bones, frontal bone, two temporal bones, sphenoid bone, and ethmoid bone [13,22].

The occipital bone is located in the lower, back portion of the skull. It is trapezoidal shaped and mostly curved. At the base, the occipital bone has a large oval shaped opening called the foramen magnum that allows the spinal cord to enter the cranium where it becomes the brain stem. Located on each side of the foramen magnum are rounded projections called the occipital condyles by which the occipital bone articulates with the axis. The internal surface of the occipital bone is divided into four fossae, or small hollows, by a cross-shaped ridge. The superior fossae are shaped to fit the occipital lobes of the cerebellum. The inferior fossae are larger and relatively smoother and conform to the shape of the hemispheres of the cerebellum [13].

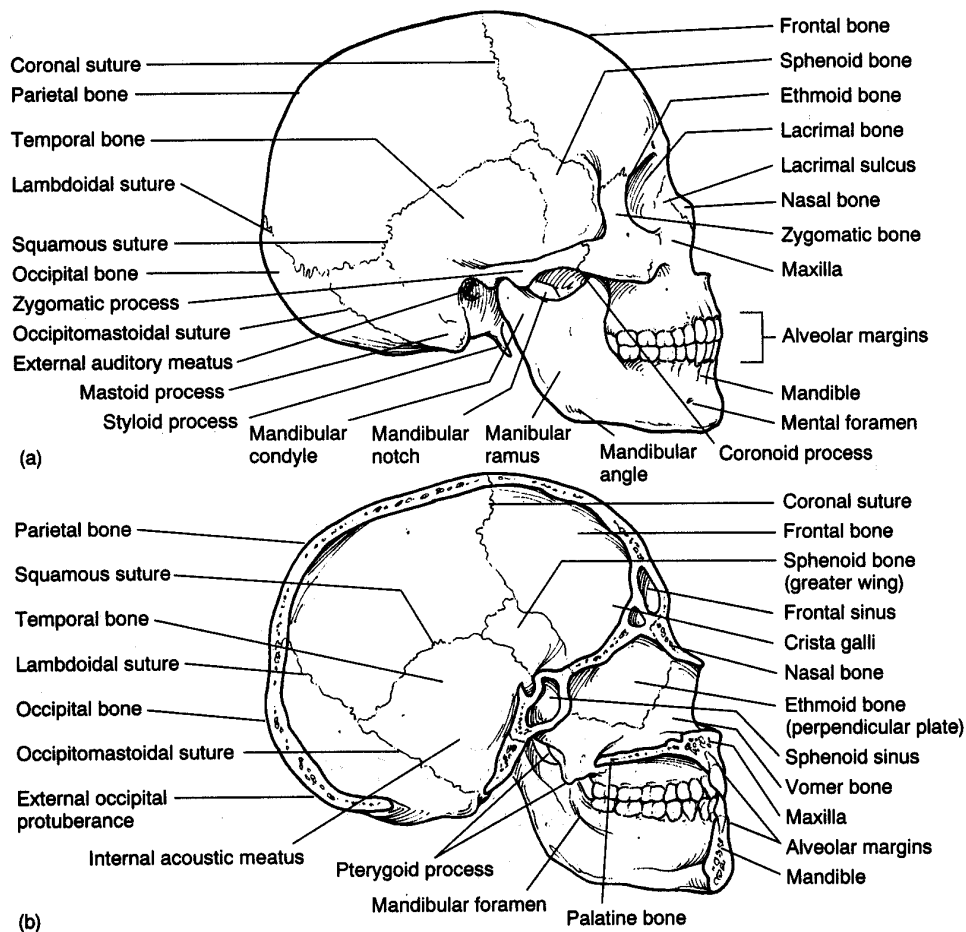


Figure 8. Side View of the Human Skull. From Ref. [2].

The two parietal bones are quadrilateral in shape and are joined at the sagittal suture to form the top and sides of the cranium. The interior surface is concave and has various shallow depressions for the convolutions of the cerebrum [13].

The frontal bone consists of two portions. The vertical portion forms the forehead and the horizontal portion forms the roof of the orbits and nasal cavities. The internal surface of the forehead has a vertical groove for superior longitudinal sinus and facilitates attachment

of the falx cerebri membrane. The horizontal and vertical internal surfaces also have various depressions for the convolutions of the frontal lobes of the brain as well as furrows for arteries. It is also the site of the frontal sinus where air circulates for conditioning [2,13].

The temporal bones are located at the sides and base of the skull. It is irregular in shape and includes the three portions. The squamous portion is flat except for with the protrusion of the zygomatic process (side of cheek bone) emerging from its base. The mandibular fossa, a depression for articulation of the process of the jawbone, is also located on this portion. The mastoid portion provides various sites for muscle attachment. The petrous portion is very dense and hard and is located at the base of the skull between the occipital and sphenoid bones. The interior surface forms the base of the rear portion of the middle fossa and the front portion of the posterior fossa [13].

The sphenoid bone, well known for resembling a bat with its wings extended, is located at the anterior part of the base of the skull. The center portion provides support for the pons. The pituitary gland lies in a saddle shaped depression on the top portion called the sella turcica. The greater wings are curved and form part of the middle fossa of the base of the skull and have depressions for the convolutions of the brain. The lesser wings support part of the frontal lobe of the brain. The sphenoid also articulates with all the other cranial bones and provides several muscle attachment sites [13]. Details of the sphenoid bone are depicted in Figure 9.

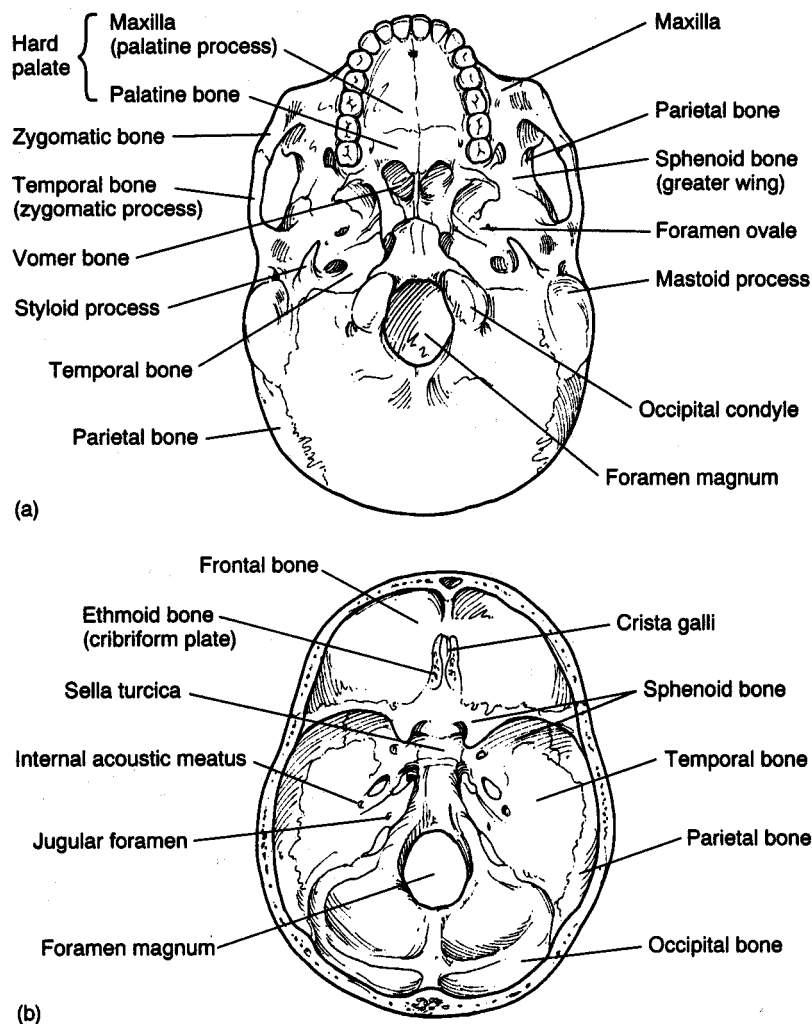


Figure 9. The Human Skull: (a) Inferior and (b) Superior View, with Cranium Removed. From Ref. [2].

The ethmoid is a light, spongy, cubical shaped bone. It is situated at the anterior part of the base of the cranium between the orbits separating the nasal cavity from the remainder of the cranium. The olfactory nerves pass through holes in the ethmoid process to enter the brain. These holes occur in two thin horizontal plates called the cribriform plates. A triangular process called

the crista galli projects upward between the cribiform plates. These features are shown in Figure 9 (b). There are no muscles attached to this bone [2,13].

e. The Meninges

The brain and spinal cord are supported and protected by a group of three membranes called the meninges. One function of the meninges is to isolate the brain and spinal cord from the surrounding bones. The three layers of the meninges are the dura mater, the arachnoid mater and the pia mater. The dura mater is the outermost layer consisting of tough fibrous connective tissue and many blood vessels and nerves. Inside the skull it is divided into two layers, one lining the inside of the skull and the other covering the brain. Folds of the dura form the falx cerebri situated in the fissure between the left and right cerebral hemispheres, and the tentorium cerebellum which forms a horizontal shelf between the cerebrum and cerebellum and vertically separates the right and left portions of the cerebellum. The arachnoid mater occupies the subdural space and is a delicate spider-web-like membrane without blood vessels. The pia mater is very thin, with many nerves and small blood vessels. The space between the arachnoid mater and the pia mater is called the subarachnoid space and contains a clear, water fluid called the cerebrospinal fluid (CSF) which provides nutrients and cushioning from shock for the brain. The cerebrospinal fluid continuously circulates through the ventricles and subarachnoid space in the brain and along the spinal cord. For normal movement, any shrinkage or expansion of the brain is compensated by movement of CSF between the brain

and spinal cord spaces [2,22]. Details of the meninges are illustrated in Figure 10.

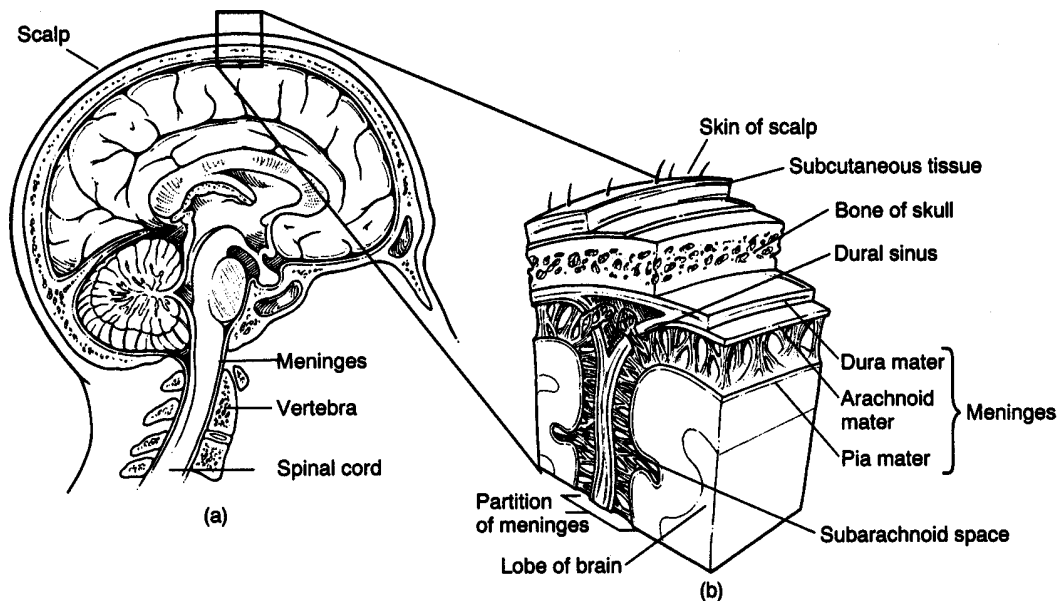


Figure 10. Structures Enclosing the Nervous System. (a) Relationship of the Brain and Spinal Cord to the Bones that Enclose them. (b) Details of the Three Layers of the Meninges. From Ref. [2].

d. The Brain

The adult human brain is a mass of jellylike tissue made up of approximately 100 billion nerve cells, supporting tissue; vascular and other tissues. The average weight of the brain is approximately 1.36 kg (3.0 lbs). The average length is about 165 mm (6.5 in) and its greatest transverse diameter is about 140 mm (5.5 in) [22,30].

The outer portion of the brain is made up of the cell bodies of neurons that are referred to as gray matter. The inner portion is composed primarily of axons with myelin sheaths that are referred to as white matter [2].

The brain can be divided into three basic parts: the cerebrum, the cerebellum, and the brain stem. Additionally, the brain stem is composed of several structurally significant parts: the diencephalon, the midbrain, the pons, and the medulla oblongata. The brain also has four ventricles, 3 membranes (meninges), 2 glands (pituitary and pineal), 12 pairs of cranial nerves, and the cranial arteries and veins [22]. The main features of the brain are shown in Figure 11.

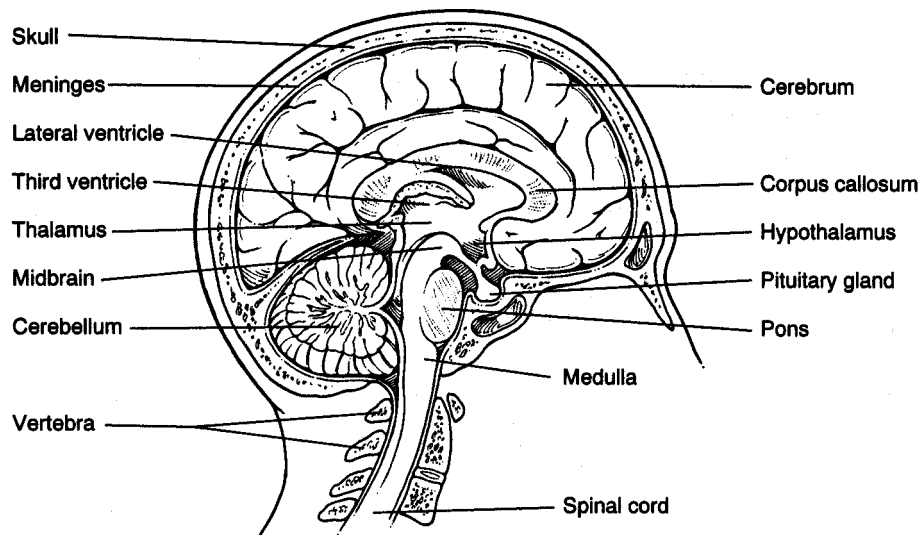


Figure 11. The Human Brain in Position in the Skull as Seen from the Lateral Aspect. From Ref. [2].

A series of interconnected cavities known as the ventricles lie within the cerebral hemispheres near the center of the brain. Two lateral ventricles are located within cerebral hemispheres, the third ventricle is located near the corpus callosum and the fourth ventricle is located in the brain stem. Cerebrospinal fluid fills the ventricles, covers the entire brain in the subarachnoid space, and flows into the central canal of the spinal cord. The cerebrospinal fluid protects the internal portion of the brain from varying pressures [2,30].

The cerebrum is the largest part of the brain and is divided into right and left cerebral hemispheres. The cerebral hemispheres are separated by a deep midline cleft called the longitudinal fissure. At the base of the longitudinal fissure, a bridge of nerve fibers called the corpus callosum connects the two cerebral hemispheres. The surface of the cerebrum, referred to as the cerebral cortex, is composed of numerous convolutions, or folds. The ridges of the folds are called gyri, and a shallow groove is called a sulcus whereas a deep groove is a fissure. The interior of each cerebral hemisphere is composed of white matter. Each cerebral hemisphere is further subdivided into four lobes by fissures, each lobe being named by its association to the nearest cranial bone. The frontal lobe is located at the anterior portion. The parietal lobe lies posterior to the frontal lobe and is separated from the frontal lobe by the central sulcus. The temporal lobe is located below the frontal lobe and is separated by the lateral sulcus. The occipital lobe is located at the posterior portion of the lateral hemisphere. An additional part of the brain called the insula, is

covered by portions of the frontal, parietal and temporal lobe [2,22,30].

The cerebellum is located at the lower back of the brain beneath the occipital lobes and behind the pons and medulla oblongata. It consists of two lateral hemispheres that are separated by a layer of dura mater called the tentorium. The tentorium also separates the cerebrum from the cerebellum on top. The cerebellar hemispheres are joined at the midline by a narrow bundle of white fibers called the vermis. The outer cortex of the cerebellar hemispheres is gray matter; the inner cortex is white matter. The outer surface of the cerebellum forms into narrow folds separated by deep fissures. Three pairs of nerve fiber bundles called the cerebellar peduncles connect the cerebellar hemispheres to the midbrain, pons, and medulla oblongata [22,30].

The brain stem connects the cerebrum to the spinal cord and contains a number of structures. The main structures of the brain stem include the diencephalon, the midbrain, the pons, and the medulla oblongata.

The diencephalon lies between the midbrain and the cerebral hemispheres and encloses the third ventricle. It is organized into masses of gray matter called nuclei. The thalamus and the hypothalamus lie underneath the cerebrum and connect it to the brain stem. The thalamus consists of two rounded masses of gray tissue lying within the middle of the brain, between the two cerebral hemispheres. The thalamus acts as a relay center for incoming sensory signals to the cerebral cortex and for outgoing motor signals from it. Another nucleus of the

diencephalon is the hypothalamus which sends impulses to and receives them from the cerebrum and thalamus. The hypothalamus lies beneath the thalamus on the midline at the base of the brain [30].

The midbrain is located between the pons and the diencephalon. Nerve fibers of the midbrain connect the cerebral hemispheres to the brain stem and spinal cord. Nerve cells within the midbrain function as relay centers. Corticospinal tracts connecting the cerebrum and spinal cord are found on the underside of the midbrain. Within the midbrain is the cerebral aqueduct that connects the third ventricle above to the fourth ventricle below [22].

The pons is an egg shaped bulge that lies below the midbrain in front of the cerebellum, and above the medulla oblongata. The pons consists of large bundles of white matter nerve fibers that connect the two halves of the cerebellum and also connect each side of the cerebellum with the opposite-side cerebral hemisphere. The nerve fibers of the pons relay impulses to the cerebrum and back to the medulla oblongata [30].

The long lowermost portion of the brain stem is called the medulla oblongata. It is continuous with the pons and the midbrain above and makes a gradual transition into the spinal cord, below at the foramen magnum. All ascending and descending nerve fibers pass through the medulla oblongata. In the lower part of the medulla oblongata, motor fibers cross from one side to the other so that fibers from the right cerebral cortex pass to the left side of the body. The medulla also contains a network of nerve fiber called the reticular formation. It runs up the

brain stem from the medulla oblongata through the pons and the midbrain. Nerve fibers in the network are responsible for activating the cerebral cortex when sensory impulses are received [30].

B. LITERATURE REVIEW

Several 2D and 3D models have been developed over the past 30 years but few have been fully validated. The models have ranged from simple spherical shell and fluid models with linear elastic material properties to complex, three-dimensional, geometrically correct models with viscoelastic, nonlinear properties. These models have provided insight into brain injury mechanisms and postulation for injury tolerance criteria.

Ward and Thompson developed one of the first successful finite element models for investigation of head injury [34]. Their model was a three dimensional representation of the cerebrum, cerebellum, brain stem, ventricles, falx cerebri and tentorium cerebelli. The material properties of the brain were modeled as linear elastic. With their model, Ward and Thompson demonstrated the importance of modeling the tentorium and falx cerebri by comparing results with and without the membranes. With the membranes included, the model correlated well with static and modal experimental data.

Ward later revised the previous model to include a meshed skull and new material properties [24]. The new model was validated by comparing the model response with cadaver head impact test data. Measured and computed pressures were compared at five locations in the brain. There was good agreement throughout except opposite the

impact site, where the magnitude of the measured negative pressure was lower than the computed stress. The model also exhibited the positive pressure at impact site and negative pressure at the contrecoup site, thus confirming experimental observation.

Ward revised the model again and used it to simulate cadaver impact tests and real aircraft accidents [35]. The new model included new material properties where the Poisson's ratio of the brain was varied according to impact duration to simulate the pressure release mechanisms or volume elastance. Brain injury severity was correlated with peak intracranial pressure. The results showed that serious and fatal injuries occur when the pressures exceed 34 psi (234 kPa). Based on this pressure tolerance limit a brain injury tolerance curve was proposed. A comparison is made between other injury criteria including the Wayne State Tolerance Curve, Head Injury Criteria (HIC), and Motorcycle Helmet Standard No 218.

In another paper, Ward reviewed the status of current finite element models and their applications and limitations [36]. Ward discusses the deficiencies noted in several early models and suggests three requirements that should be included in the models. First, the opening in the base of the skull, the foramen magnum, must be simulated because tissue and fluids move through the opening. It acts as a pressure release mechanism for the brain. Secondly, the falx and tentorium partition the cranial cavity and provide support for the brain and must be included in the model. Finally, the brain must not be

modeled as incompressible. A lower bulk modulus or effective Poisson's ratio must be used.

Khalil and Viano also provided a critical review of several current models to that date [15]. They identified several critical features considered major factors that compromised the accuracy of the models. Some of the most significant errors found in the models include: no provision for relative motion between the skull and brain; wide variation of fluid compressibility not corresponding to experimental values; resonant frequencies of the head were ten times too low compared with experimental values; and acceleration input not sufficiently representative of head impact. The effects of fixed, hinged, sliding and free, head-neck boundary conditions were also discussed with the conclusion that the most reasonable boundary condition probably depends on the impact condition but needs further investigation.

Troseeille et al. developed a specific experimental protocol for cadaver testing and measurement of acceleration and intracranial pressures to be used in developing finite element models [31]. The authors also discussed the influence of material properties of the brain, tentorium and cerebrospinal fluid used in finite element modeling. Additionally, they conducted impact studies using volunteer boxers as subjects. Head accelerations of the boxers were measured during training fights. The measured acceleration was applied to a 2D finite element model proposed by General Motors. For comparison, the model was modified to include the tentorium and representation of the cerebrospinal fluid as a low

shear modulus solid to allow for relative movement between the brain and skull. The objective was to establish an under-estimation of human head tolerance by relating the two models responses to observed effects on the boxers. The results were also compared to literature data. Large differences in response occurred between the two versions of the model but it was unclear whether one was preferred over the other.

Ruan et al. developed a 3D finite element model of the head that included the scalp, a three-layered skull, cerebrospinal fluid, dura mater, falx cerebri, and the brain [28]. The model was validated by comparing the model response with cadaver head impact experimental data. The validated model was then used to evaluate head impact severity due to different types of impacts. The impact speed, mass and location were varied. The model predicted higher skull Von Mises stress and higher negative intracranial pressures in the contrecoup region for occipital impacts than for frontal impacts. The authors note that this result may explain clinical observations that more severe contrecoup injuries occur with occipital impacts. The results also showed that the effect of impactor mass on head response was not as large as that of impactor velocity. Additionally, the Head Injury Criterion (HIC) was found to be proportional to intracranial pressure, brain shear stress, and skull Von Mises stress, therefore, the authors concluded that for direct head impact HIC seems to reasonably reflect impact severity.

Zhou et al. developed a detailed three-dimensional human head model as a continuation of the two-dimensional

porcine brain models by Zhou et al. (1994) and the three-dimensional human head model by Ruan et al. (1994) [39]. The model consisted of the scalp, skull, dura, falx tentorium, pia, cerebrospinal fluid, venous sinuses, ventricles, cerebrum (white and gray matter), cerebellum, brain stem, and parasagittal bridging veins. The objective was to study the importance of including the white and gray matter, ventricles and bridging veins in the three-dimensional model. The model was run with and without these features for comparison. First the model was partially validated by comparison with experimental cadaver impact tests of Nahum et al. (1977). Then a sagittal plane rotation simulation was conducted using a rotational impulse from an animal test conducted by Abel et al. (1978). The authors concluded that the model's results showed that differentiation between white and gray matter and the inclusion of the ventricles are necessary in brain modeling to predict higher shear stresses in the corpus callosum and brain stem, although the pressure response between the two models essentially remained the same. The model also predicted that the bridging veins in the central part of the superior sagittal sinus were at higher risk of rupture due to impacts. The authors concluded that the model indicated this would probably occur during the acceleration phase of occipital impacts; implying the importance of impact direction in causing subdural hematoma. It was noted that this could also explain why a low incidence of subdural hematoma occurs in vehicular accidents where frontal impacts predominate as opposed to falls and assaults where frontal impacts do not.

Bandak et al. used a simplified three-dimensional finite element model developed by Dimasi and Eppinger to study the evolution of strain in the brain under impulsive acceleration loadings [4]. The model consisted of a rigid skull, dura mater, falx cerebri and upper portion of the brain. A Cumulative Strain Damage Measure (CSDM), based on the volume fraction of the brain that has experienced a specific level of stretch, was proposed by the authors as a possible indicator for deformation related brain injury. Specifically, this measure was proposed as a possible predictor for strain related neural damage known as Diffuse Axonal Injury (DAI) resulting from head impact. This damage measure was used to evaluate the relative effects of rotational and translational accelerations on the development of strain damage in the brain. The model was subjected to different combinations of translational and rotational accelerations that might be expected to result from automotive crash restraint system forces. The authors found that the damage measure values were associated mostly with rotational accelerations which also agrees with experimental findings. Additionally, the model showed that anterior-posterior rotations appeared to be somewhat more severe than medial-lateral rotations.

Dimasi, Eppinger and Bandak used the previously mentioned model again in another study where HIC was compared to their proposed CSDM as a predictor of DAI [8]. Accelerometer data was used to replicate the translational and rotational dynamic loads experienced during actual crash testing and applied to the finite element model. The results again showed that CSDM was influenced more by rotational accelerations. Since HIC accounts for

translational accelerations only it was not a viable predictor of rotationally induced strains and resulting DAI. Therefore, it was shown that CSDM accounts for soft tissue brain injuries that are not detectable by HIC.

Turquier et al. conducted a validation study of a three-dimensional head model against cadaver impact tests [32]. The objective of their study was to evaluate the basis of assumptions involved in three-dimensional modeling of the head. The model was developed by coauthor Willinger using horizontal MRI slices. The model included a rigid, enclosed skull, falx, tentorium, subarachnoid space, cerebrum, cerebellum and brain stem associated with the corpus callosum. The model response matched experimental data in terms of trend but presented significant oscillations and a symmetrical coup and contrecoup pressure in the simulation that is not observed experimentally. The model was run using both linear elastic and viscoelastic material properties for the brain. It was found that the viscoelastic properties reduce the oscillations somewhat but the vibrations were more heavily influenced by the subarachnoid space Young's modulus. Better agreement with experimental data was obtained when the original Young's modulus of the subarachnoid space proposed by Willinger was replaced with the value used by Ruan (1993). The authors also suggest that the difference in pressures may be reduced by reconsidering the enclosed rigid skull assumption.

Kang et al. developed a new three-dimensional model from the basis of what was learned from the model of Turquier et al. [14]. The new model included a more

realistic geometry and more refined mesh than the previous model. The model included the skull, falx, tentorium, subarachnoid space, scalp, cerebrum, cerebellum, and brain stem. The model was validated against the cadaver impact tests of Nahum et al. (1977). Then it was used to simulate an actual motorcycle accident. Good agreement was found for the model validation as well as the intracranial shear stress distribution and observed contusion in the motorcycle accident simulation.

Claessens et al. developed two versions of a three-dimensional head model [7]. The first one modeled the skull and brain as coupled, homogeneous structures. The other, decoupled the skull and brain by prescribing a contact algorithm at the skull-brain interface. Also in the second model, the brain was modeled with additional substructures including the falx cerebri, tentorium, cerebrum, cerebellum and brainstem. The models were validated on the basis of modal analysis and by comparing model response with cadaver impact tests conducted by Nahum et al. (1977). Modal validation agreed well with various experimental and numerical data. For the impact simulation, better agreement was found with experimental data from the model with substructures. The authors believed this was because the supportive and separating function of the tentorium and falx cerebri resulted in lowering the pressures at the contrecoup site. A parametric study was conducted to determine the effect of Young's modulus of the brain. It was found to have a significant influence. If the modulus was too low, significant oscillations and over prediction of pressure occurred. The authors also concluded from the study that allowing

relative motion between the skull and brain in the model was important. The true behavior of the interface was believed to lie somewhere between the fully coupled and free interface but closer to the free interface case.

Miller et al. conducted injury-causing experiments on miniature pigs and developed two versions of a two-dimensional plane strain model of the pig to be used in conjunction with the experimental data for analysis of DAI [23]. Two approaches were used to model the interface between the skull and the brain. The first model represented the subarachnoid space (CSF) as a low shear modulus, nearly incompressible solid. The second model represented the relative motion as a sliding frictional interface. Both models included distinction of white and gray matter, the general fissure and sulci structures, the dura mater, ventricles and subarachnoid space. In a separate study, a comparison was made between a two-dimensional plane strain model of the brain's midsection and a three-dimensional model with the same frictional interface. Both models produced similar estimated strain histories and kinematic responses thus supporting the plane strain idealization used in the present study. The significant finding from the modeling includes that the mechanical response is significantly affected by the manner in which the relative motion between the cerebral cortex and the dura mater is represented. Predicted topographic distribution of axonal injury and cortical contusions were best developed when modeling the subarachnoid space as a sliding frictional interface. The maximum principal nominal strain and Von Mises stress based indices predict comparable patterns of axonal and macroscopic hemorrhagic

cortical contusion; negative pressure was a poor predictor for both forms of injury.

One of the most detailed models to date is a three-dimensional finite element model developed by Al-Bsharat et al. [11]. The model is a modified version of the previous one developed by Zhou et al. [39]. In the new model, the quality of the mesh was improved and the skull was modeled as a three-layered solid. Different linear viscoelastic material properties were assigned to the gray and white matter. The CSF remained as a low shear modulus solid but a sliding interface was introduced to simulate the interaction between the CSF and pia mater. The objective of the study was to examine both brain motion and pressure response due to blunt head impacts. Measurements of the relative motion occurring during impact between the brain and skull of cadavers was achieved. The finite element model was able to reasonably predict the trends of the motions that were observed experimentally.

Four different models, ranging from a simple solid skull to a two-layered skull filled with cerebrospinal fluid material with inclusion of representation of the head-neck joint, were developed by Mehta et al. [21]. Although the models were not yet fully validated, these models confirmed the coup-contrecoup mechanism and provided valuable insight into modeling parameters and possible head injury mechanisms.

More recently, Krabbel and Muller have developed a promising, highly realistic three-dimensional head model using digital CT and MRI data obtained from the Visible Human Project Data set [17]. The model includes a

geometrically detailed skull and brain. Preliminary comparison with experimental impact test data resulted in good correspondence in terms of contact force, center of gravity acceleration and dynamic motion.

THIS PAGE INTENTIONALLY LEFT BLANK

III. HEAD INJURY

A. TYPES AND BIOMECHANICAL MECHANISMS OF HEAD INJURY

Head injuries can be grouped into three general categories: external soft tissue, skull injury, and brain injury [9]. Although, brain injuries are much more serious than skin or skull injuries. For this study, brain injury is of primary concern; therefore, the possibility of soft tissue injury and skull fracture will not specifically addressed.

Brain injuries can occur due to rapid momentum change resulting from direct contact forces to the head or from non-contact inertial forces transmitted through the neck. The human head is one of the most vulnerable parts of the human body when subject to large impact and inertial loading [4,9].

Traditionally, it has been viewed that head injury is caused by the translational and rotational accelerations of the head produced by an impact. In reality the vast majority of head injuries are generated from both translational and rotational inputs. The type and severity in general, depends on the magnitude and duration of the translational and rotational inputs. Injuries commonly associated with translational inputs are skull fracture and cerebral contusions (coup and contrecoup) while the injuries associated with the rotational inputs are bridging vein tears and diffuse axonal injury [29]. More recently, researchers have argued that acceleration, per se, is not the proximate cause of injury, rather, rapid motions of the skull causes displacement of the hard bony structures of

the head against soft tissues of the brain which lag in their motion due to inertia and loose coupling to the skull [33]

Closed head impact can result in a wide range of injury types and locations within the cranium. Brain injuries can be subdivided into two broad categories: diffuse injury and focal injury. Diffuse brain injury, which consists of brain swelling, concussion, and diffuse axonal injury (DAI) can be identified by microscopic evaluation of neural tissue. Focal injuries are primarily observable vascular hemorrhage and contusion of the brain tissue, and include epidural hematomas, subdural hematomas, intracerebral hematomas, and contusions (coup and contrecoup). Focal brain contusion injuries are related to adjacent bony tissues and stiff membranes, particularly the grooves of the anterior and middle fossae supporting the frontal and temporal lobes [4].

Studies have shown that diffuse injuries are more common in victims of auto accidents while focal injuries are most often found in victims of assault or falls. Of these injuries, acute subdural hematoma and diffuse axonal injury were the two most important cause of death [22].

1. Diffuse Injury

Diffuse Injuries form a spectrum of injuries ranging from mild concussion to diffuse white matter injuries. In the mildest forms, there is mainly physiological disruption of brain function and, at the most severe end, physiological and anatomical disruptions of the brain occur [22].

Mild concussion does not involve loss of consciousness. Confusion disorientation and brief duration of posttraumatic and retrograde amnesia may be present. It is the most common form of diffuse brain injury and is completely reversible [22].

Classical cerebral concussion may be defined as an immediate loss of consciousness following a change in kinetic energy. The loss of consciousness is usually less than 24 hours. Unconsciousness can occur when the ascending or descending tract of the reticular formation located along the length of the brain stem is interrupted, or the reticular formation itself is injured. Amnesia and additional associated injuries may also be present. Cerebral concussion can result from whiplash as well as a direct blow to the head [9].

Concussion is most likely related to shear strain since the strains are high in the regions controlling consciousness and memory [36]. At the same time, pressures in these regions are usually low. As a result of impact and the resulting relative motion between the brain and skull, the main cerebral mass may rotate in relation to the brain stem. This puts an intermittent stretch on the reticular formation [9]. The stretching in the brain stem region can result in instantaneous unconsciousness due to the disruption of impulses to and from the reticular formation. The relative motion between the brain and skull produces trauma to the brain as well as tearing of the blood vessels that connect the brain to the overlying membranes [9].

More than one mechanism is postulated to be the cause of concussion. The response characteristics thought to be the causes of concussion are: pressure differentials in the brain, flexion extension and bending of the upper cervical cord, relative displacement between the brain and skull producing contrecoup injury or cavitation, shear stresses in the brain stem near the foramen magnum, shear stresses in the upper brain stem due to angular displacement, and pressure waves traveling in the brain [34]. For head impacts most of these characteristics are present, each being a partial description of the reaction of the brain and spinal cord.

Diffuse Axonal Injury (DAI) is a brain injury that occurs when the axons of neurons are stretched and torn, producing cell death or the mechanical disruption of many axons in the cerebral hemispheres and subcortical white matter [22]. DAI is concentrated in the deep cerebral regions and is not visible on radiological exams. DAI observed in more than 50% of all head injury cases with symptoms ranging from mild or temporary short lived loss of consciousness to severe long duration deep coma that results frequently in death. Lesser degrees of DAI can result in reversible comas: not all of the axonal disruption associated with DAI is irreversible [4]. Although not completely understood nor accurately predicted, the nature and consequences of DAI are now postulated as mechanical damage that is proportional to both the magnitude and rate of strain occurring in the brain. Axonal injury is thought to depend on a number of factors including the location of injury, the magnitude of strain induced, and the volume of the brain material

affected. These factors, in turn, are influenced by the magnitude and direction of the applied dynamic loading [8].

Shearing injuries are another form of diffuse brain injury. Shear strains are the largest strains in the brain. The high shear strain regions are in the brainstem and cerebellum and along the external surface of the cerebral cortex [36]. In addition to causing hemorrhage, subdural hematoma and concussion, shear strain is the most likely cause of laceration. Laceration is the most severe form of brain injury and occurs when the brain is subjected to a force of sufficient intensity to cause a tearing and disruption of the brain substance itself. Injuries, in general, are more severe where shear strain and tension stress combine.

Brain swelling, or an increase in intravascular blood within the brain, may be superimposed on diffuse brain injuries, adding to the effects of the primary injury by increased intracranial pressure [22].

2. Focal Injury

Acute subdural hematoma occurs in nearly 30% of severe head injuries. It usually causes a marked increase in intracranial pressure and serious deformation of the brain. Consequently it is associated with a high mortality rate, 57-90%. In closed head impact, subdural hematomas can be caused by brain laceration or contusions, or tearing of the bridging veins. However, bridging veins rupture is the primary cause. When relative motion occurs between the brain and skull, such as during head impacts, the veins can be stretched and torn [19].

Cerebral contusion is defined as bruising of the brain without a break in the continuity of the surface or deeper tissues. They are usually visible on a CT scan. Contusions are often located in the superficial brain structures, often close to the skull, but sometimes deep cerebral hematomas occur and always coexist with DAI. Contusions occur not only at the site of impact and in the areas of contrecoup damage, but may be sufficiently widespread to constitute a form of diffuse brain injury. In the region of the impact (coup), pressure from the blow causes small blood vessels to burst. As the energy wave is transmitted through the brain substance, various other small vessels are disrupted and hemorrhages occur. The contrecoup lesions are more significant than the coup lesions. They occur predominantly at the frontal and temporal poles, which are impacted against the irregular bony floor of the frontal and middle fossae.

In the contrecoup area the mechanism of hemorrhage is more complex. As the relatively rigid skull is driven forward, the brain deforms and lags behind compressing against the skull creating a positive pressure region at the coup site. A negative pressure region is created at the contrecoup site as the skull pulls the brain along. The negative pressure forms gas bubbles in and on the brain substance, which cause injury during both formation and collapse. Small blood vessels in the surrounding areas are simultaneously subjected to negative pressures that cause blood to leak into brain tissue, at the same time, a surface wave travels along the brain periphery toward the area of negative pressure. When this wave reaches the outer area of cavitation, there is a forward projection of

the surface brain tissue and a whipping motion takes place, subjecting the area to even more injury [9]. Body tissues tolerate positive pressure better than negative pressures; hence, the contrecoup injury is often more severe than the coup injury. High, nearly hydrostatic normal stresses are thought to be the primary cause of contusions. Compressive stresses of 234 Pa (34 psi) can cause serious brain trauma near the impact site. Tension stresses of 186 Pa (27 psi) can cause contrecoup contusions opposite the impact site [36].

B. HEAD INJURY CRITERIA

Determination of human tolerances to injury is complicated by a number of factors, including the magnitude, distribution, duration and pulse shape of force of the impact; the body orientation, characteristics of the striking object. Biological factors may also influence human tolerance including sex, age, physical and mental condition, body size. Variation between individuals must be considered because tolerance under certain conditions can vary from one person to the other. Additionally, current tolerance criteria are based on the occurrence of a single impact event. Less is known about the effects of multiple impacts occurring at different locations.

The Head Injury Criterion (HIC) is currently used to evaluate the severity of head injuries sustained in automobile accidents. The Federal Motor Vehicle Safety Standard (FMVSS) 208 defines HIC by the following equation:

$$HIC = \left[\frac{\int_{t_1}^{t_2} A(t) dt}{t_2 - t_1} \right]^{2.5} \quad (t_2 - t_1) = 1000$$

Where A(t) is the time history of the resultant acceleration of the center of gravity of the head in Gs, and t2 and t1 are time points that are varied to maximize HIC []. The National Highway Traffic Safety Administration established a HIC tolerance limit of 1000. Another index that used in conjunction with HIC is the Abbreviated Injury Scale (AIS). AIS is a coding system used to classify injury severity as shown in Table 1. HIC equal to 1000 corresponds to a 16% risk that severe (AIS 4) head injury may occur [18]. A curve indicating the risk of life threatening brain injury as a function of HIC is given in Figure 12.

AIS	Severity Code
1	Minor
2	Moderate
3	Serious
4	Severe
5	Critical
6	Virtually unsurvivable

Table 1. Abbreviated Injury Scale Severity Codes. From Ref. [18].

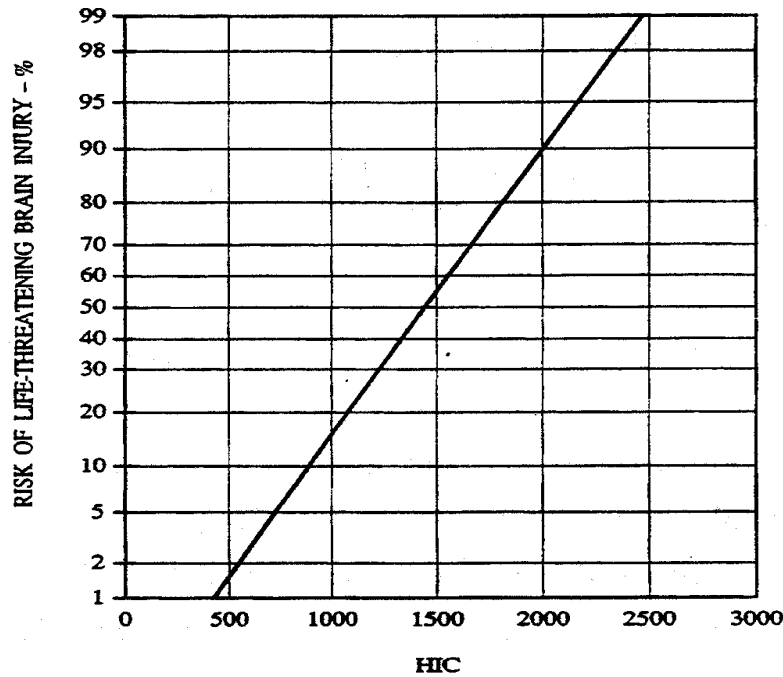


Figure 12. Injury Risk Curve for HIC. From Ref. [18].

The Head Injury Tolerance curve originated from the Wayne State Tolerance Curve which was based on data from experimental impact tests conducted on animals and cadavers by Lissner et al. (1960). The curve was originally a plot of the effective head acceleration versus time duration from unembalmed cadaver impact tests conducted for time durations of 1 to 6 ms [26]. The curve was later extended to time durations above 6 ms using comparative animal and cadaver impact data with human volunteer sled acceleration tests [22]. In 1961, Gadd fit the WSTC data, plotted on a log-log scale, with a straight line. Gadd subsequently used this to develop an acceleration-weighted impulse criterion called the Gadd Severity Index (GSI). This index was widely used in crash injury research until the National Highway Traffic Safety Administration rescinded its use as

a result of certain objections. The GSI was supercede by the Head Injury Criterion which was the same as the Gadd Severity Index except the "effective acceleration" was replaced by the conventional average waveform level for acceleration where the integration is carried out over the full time duration of the impulse. HIC was later modified to its current definition by stipulating that the time points spanning the impulse should be chosen such that HIC is maximized [26].

C. OTHER PROPOSED INJURY TOLERANCE CRITERIA

Numerous other head injury criteria have been proposed over the last few decades. While many of these were based on the WSTC, there have been several other notable attempts to develop criteria which are independent of the WSTC. Although some of these criteria appear to be reliable predictors of certain types of head injury; they are yet to be universally accepted.

One of the early models was proposed by the Vienna Institute. The criterion based on the maximum displacement of a simple, single degree-of-freedom model. Another single degree-of-freedom model was suggested by the Highway Safety Research Institute (HRSI) at the University of Michigan called the Maximum Strain Criterion (MSC). The MSC was derived from the differences in acceleration between the front and back of the skull [35].

Ward proposed a Brain Pressure Tolerance (BPT) curve based on the occurrence of brain contusion and hemorrhage derived from the combined predictions from a finite element model of the head and experimental data [35]. Ward determined that intracranial pressures above 34 psi could

produce brain contusions. Curves of the head acceleration that produces 34 psi were proposed as tolerance limits.

Dimasi et al. [8] also proposed a finite element model based criterion called the Cumulative Strain Damage Measure (CSDM). The measure estimates damage to the soft tissues of the brain by accounting for the strains induced by translational and rotational kinematics.

THIS PAGE INTENTIONALLY LEFT BLANK

V. FINITE ELEMENT MODEL

A two-dimensional, plane strain, finite element model of the head and spine was developed that is capable of adequately predicting the biodynamic response of head injury due to impact. The model includes the cervical vertebrae, intervertebral disks and facet joints along with, the skull, and major components of the brain including the cerebrum, cerebellum, brain stem, tentorium and the surrounding cerebral spinal fluid. The commercial finite element package MSC/PATRAN was used for pre and post processing and MSC/NASTRAN was used for analysis.

A. SPINE

The model of the cervical spine was based on the model developed by King [16] who based his model on a previous one developed by Williams and Belytscho [38]. Since a different analysis program was used than that of King, some element types were not available and the model had to be modified. The spine is modeled with a series of beam elements. Each vertebra is modeled with two beam elements. The intervertebral disk between the vertebrae is modeled with one beam element. Two beam elements are used to model the facet joint with the end of each beam connected to the midpoint of an adjacent vertebra [16]. The head-neck joint was modeled using two beam elements connected in a V-pattern. The material properties of the spine model are listed in Table 2.

Component	Young's Modulus E [Pa]	Poisson Ratio ν	Density ρ [kg/m ³]
Vertebrae	1.213×10^{10}	0.2	1000
Disks	1.5×10^9	0.2	100
Facet Joints	1.5×10^4	0.2	1000
Head-Neck joint	1.213×10^8	0.2	1000

Table 2. Material Properties of the Cervical Spine Used in Model.

The entire spine was modeled in a similar fashion as the cervical spine and was used to facilitate simulation of the sled acceleration test used for the dynamic validation of the head-neck. For subsequent head-neck analysis only the cervical portion of the spine and the first thoracic vertebra will be retained.

B. HEAD

The finite element model of the head is a geometrically true representation of the head developed from sagittal plane CT images of the head obtained from Bo [6] and cross-sectional views from Olson [27]. The model includes the main anatomical features of the head including the cerebrum, cerebellum, brain stem, tentorium and the surrounding cerebral spinal fluid.

The finite element mesh of the head is continuous and represents an average adult human head. The skull is

modeled as a single layer of variable thickness, with equivalent Young's modulus, to simulate the inner spongy bone and outer cortical layers. The foramen magnum was modeled by including an opening at the base of the skull. The components of the brain: the cerebrum, cerebellum and brain stem are all modeled as two-dimensional solid, plane strain elements. The brain is completely surrounded by elements representing the subarachnoid space. The subarachnoid space has been approximated as consisting entirely of cerebral-spinal fluid. The cerebral spinal fluid is modeled as a low shear modulus, nearly incompressible, solid in order to allow relative motion between the brain and skull. The tentorium is modeled using rod elements and is attached to the back of the skull and separates the cerebrum and cerebellum.

All material properties used in the model are linear elastic since the finite element package used did not allow definition of viscoelastic properties. Selecting proper material property values for biological material is always difficult. Since biological material is nonlinear, anisotropic, and often viscoelastic. The Material properties found in the literature vary widely. Averages of the most frequently used values from the literature were used for this study. A comparison of the various material properties used by other researchers is shown in Table 3. The material properties selected for this study are shown in Table 4. The entire head-neck model is shown in Figure 13.

Component	Bulk Modulus	Young's Modulus E [Pa]	Poisson Ratio ν	Density ρ [kg/m ³]	Reference
Brain		6.8e3	0.48	1040	Ward 1975
Brain Stem		1.02e4	0.48	1040	
CSF		.1	0.48	1040	
Dura		3.213e6	0.48	1133	
Skull		5.66e9-12.3e9	0.22	1400	Shugar 1977
Fluid		21.9e8			
Scalp		3.45e7	0.4	1200	Khalil and Hubbard 1977
Shell		8.5e6	0.2	2070	
Fluid	21.9e8		0.5	1030	
Brain	4.5e6				Ward 1977
Brain Stem	2.2e5				
Brain		6.67e5	0.48-0.499	1040	Ward 1980
CSF		6.67e4-6.67e5	0.48-0.4999	1040	
Skull		4.46e9	0.21	1400	Hosey and Liu 1980
CSF		6.67e4	0.49-0.49999462	1040	
Brain		6.5e5	.48-.499		Ward 1982
Membrane		3.15e7	.45		
Skull		4.46e9	.21		
Brain		2.4e7-2.4e8	0.49		Troseille 1992
CSF		G=0.2e3	0.49999		
Membrane		1.0e8			
Brain	1.86e9				Bandak and Eppinger 1994
Dura mater		3.45e7	0.45		
Falx Cerebri		3.45e7	0.45		
Brain		6.75e5	0.48	1140	Zhou 1995
Subarachnoid		1.2e4	0.49	1040	
Tent/Falx		3.15e7	0.45	1140	
Brain	5.625e6				
Subarachnoid		1.445e6	0.489		
Brain	5.625e6	6.75e5	0.48	1140	Turquier 1996
Subarachnoid		1.2e4	0.49	1040	
Tentorium		3.15e4	0.45	1140	
Falx					
Skull		6.5e9	0.22	2070	Claessens 1997
Face		6.5e9	0.22	5000	
Cerebrum		1e6	0.48	1040	
Cerebellum		1e6	0.48	1040	
Falx		3.15e7	0.45	1130	
Tentorium		3.15e7	0.45	1130	
Brainstem		1e6	0.4	1040	

Table 3. Various Material Properties of the Head from the Literature.

Component	Young's Modulus E [Pa]	Poisson Ratio ν	Density ρ [kg/m ³]
Skull	6.5×10^9	0.22	2100
Cerebrum	1.5×10^6	0.48	1040
Cerebellum	1.5×10^6	0.48	1040
Brain Stem	1.5×10^6	0.4	1040
Tentorium	1.0×10^8	0.45	1133
CSF	6.67×10^3	0.49	1040

Table 4. Material Properties of the Head Used in Model.

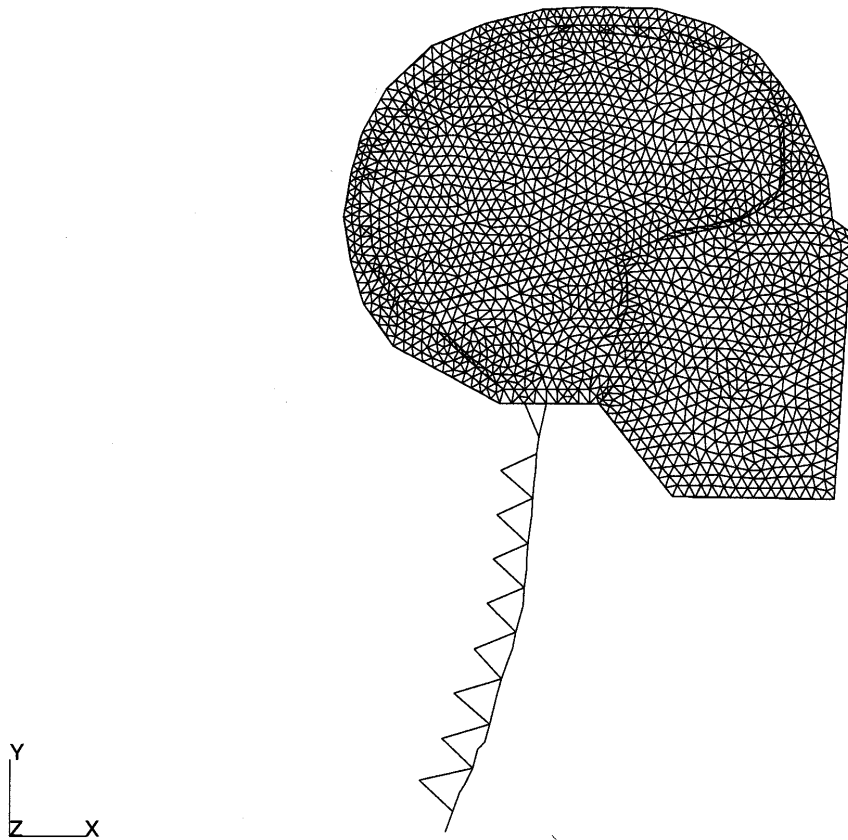


Figure 13. Finite Element Model of the Head and Neck.

V. RESULTS AND DISCUSSION

A. MODEL VALIDATION

1. Ewing Sled Test

To validate the dynamic response of the head and spine a comparison was made with the data from the Naval Biodynamics Lab (NBDL) human volunteer sled acceleration test conducted by Ewing et al. [10]. In this test, volunteers are seated in an upright position and restrained by shoulder straps, a lap belt and an inverted V pelvic strap tied to the lap belt. The head and neck are not restrained. The subjects are then exposed to short duration acceleration simulating frontal impact. The sled was linearly accelerated from rest to a maximum of 7.4G at 14.2 ms and then allowed to decelerate linearly back to rest at 340 ms. The resulting 3D displacements and accelerations of the head and first thoracic vertebral body were recorded.

a. Method and Simulation

To simulate the test, a method similar to that used by Williams and Belytscho [38] and King [16] was employed. The finite element model of the head and spine was fixed to a rigid wall with three linear springs ($k = 1 \times 10^5$ N/m) representing the sled and restraint system. A spring was attached to the first thoracic vertebra, 10th thoracic vertebra and the second lumbar vertebra as shown in Figure 14. The pelvic region was free to move in the X-direction only. The wall was then accelerated along the profile used in the sled test using the method of large mass. The resulting vertical displacement and linear

components of acceleration of the center of gravity of the head was compared with the experimental results.

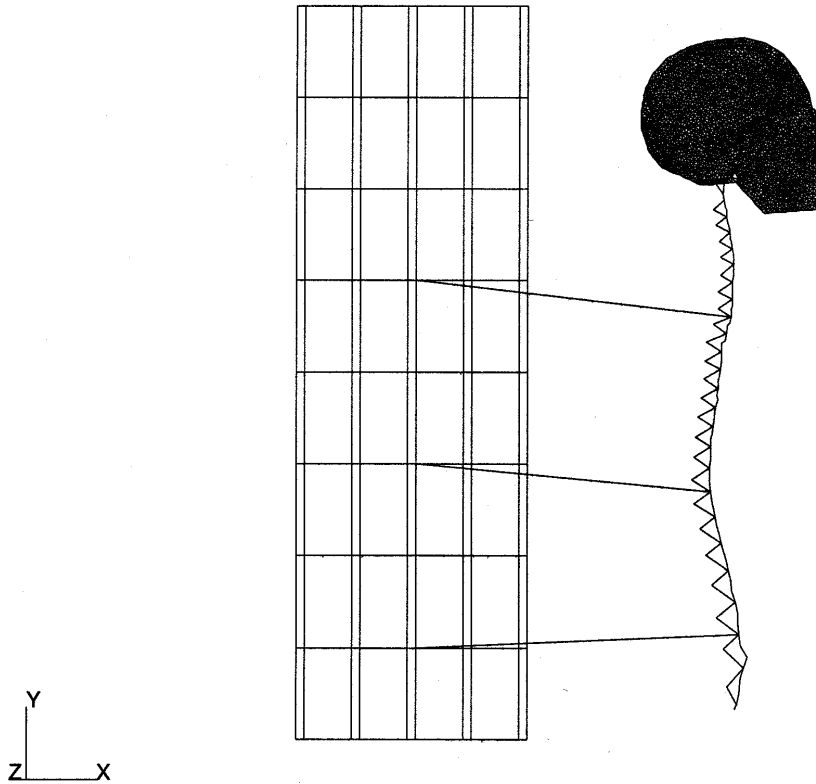


Figure 14. Finite Element Model Simulating Sled Acceleration Test.

b. Results

Figure 15. shows the vertical displacement of the head relative to the first thoracic vertebra. The model response agree well with the experimental data in terms of general curve shape and peak displacement, although the model has a slight delay in reaching the peak displacement. The response of the model shows that the head begins to drop earlier than it does in the experiment, but it also

comes back up later than in the experiment. This discrepancy is probably due to the simplicity of the neck model; since the muscles, ligaments and other soft tissue of the neck were not modeled. In reality, the neck muscles will contract shortly after the initial acceleration, thus changing the effective stiffness and damping of the neck.

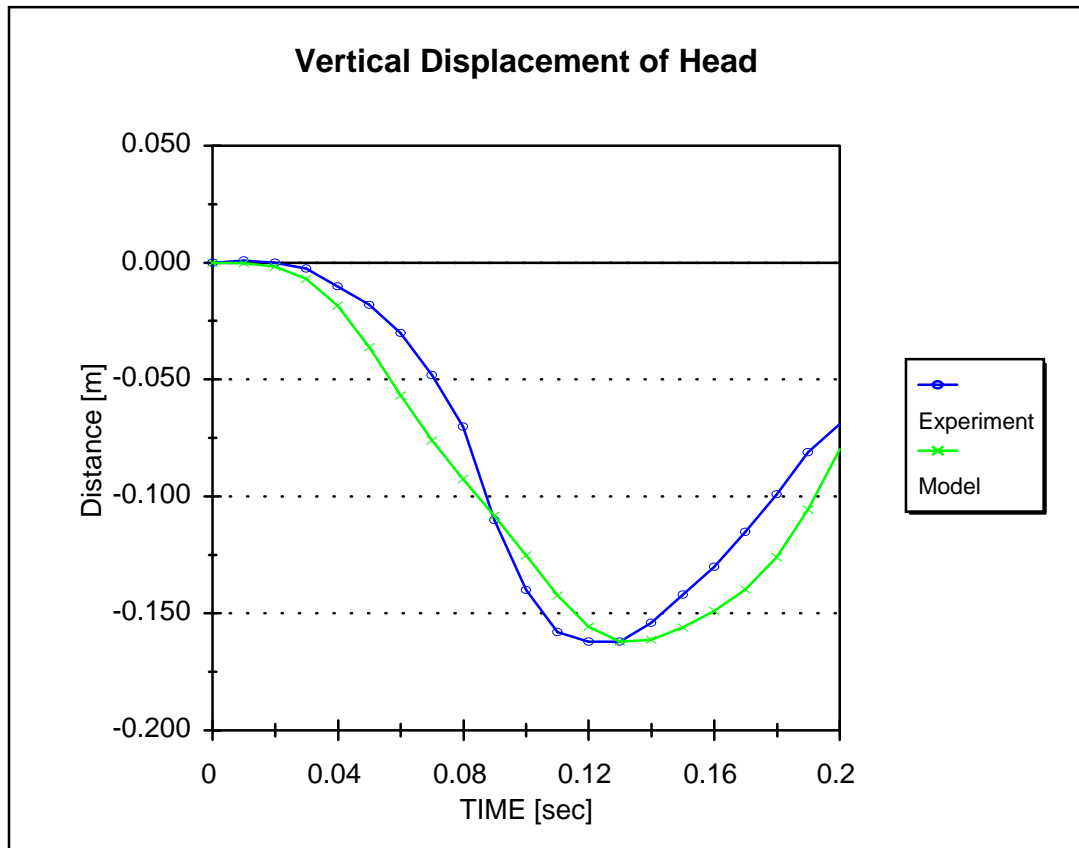


Figure 15. Vertical Displacement of the Head

The acceleration of the center of gravity of the head in the X-direction is shown in Figure 16. Correlation with the experimental data is fair, but the model under-predicts the magnitude of the first two negative peaks. A

slight leading time shift is also observed in the model response. Again, these discrepancies may be due to the simplicity of the model. Specifically, the facet joints should be modeled using discrete spring elements at their interface rather than as fixed beams of equivalent stiffness. The use of fixed beams was a modification from the original model developed by King. This modification was necessary since the discrete elements used in King's model were not available in the analysis program used for this study.

The acceleration of the center of gravity of the head in the Y-direction correlated more closely with the experimental data. Again, there is a leading time shift and the magnitude of the final peak is a bit low.

Overall, the dynamic response of the head-neck model was fair. Based on these results, it was concluded that additional details such as ligaments and muscles should be added to the model in order to improve correlation with experimental data before using the neck in a parametric study.

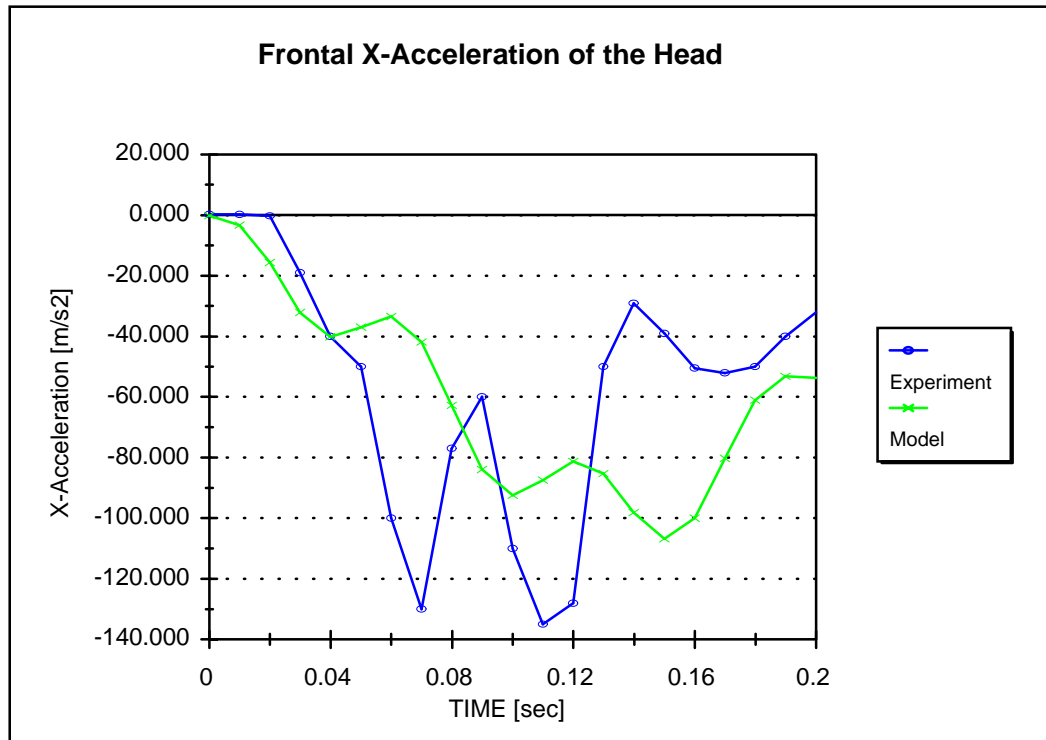


Figure 16. Head CG X-Acceleration

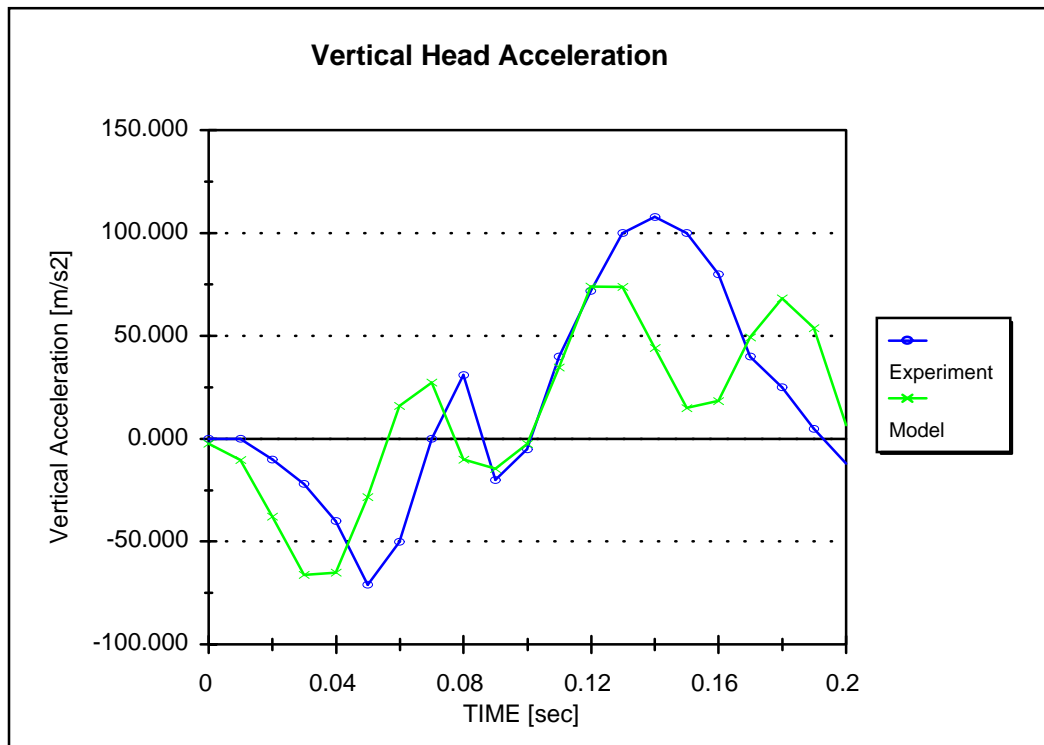


Figure 17. Head CG Y-Acceleration

2. Nahum Cadaver Head Impact Tests

Validation of the response of the head was performed by comparison with direct head impact experiments performed on cadavers by Nahum et al. [24]. In this experiment, seated, stationary cadaver subjects were impacted by a rigid mass traveling at a constant velocity. The blow was delivered to the frontal bone in the mid-sagittal plane in an anterior-posterior direction. The skull was rotated forward so that the Frankfort anatomical plane was inclined 45° to the horizontal. Various padding materials were imposed between the skull and impactor to vary the duration of the applied load. Fresh, unembalmed cadavers that were repressurized were used. In addition to the Dynamic measurements of the input force and head acceleration, a series of intracranial pressure-time histories were recorded during the experiment. The intracranial pressures were recorded at five locations: at the frontal bone adjacent to the impact contact area, immediately posterior and superior to the coronal and squamosal sutures respectively in the parietal bone, and inferior to the lamdoidal suture in the occipital bone and at the posterior fossa in the occipital bone [24].

a. Method and Simulation

To simulate the cadaver head impact experiments, the measured impact force profile was applied directly to the frontal bone of the skull at an angle of 45° from the Frankfort plane as in the impact tests conducted by Nahum. A free boundary condition is used since for short impacts it has been determined that the neck restraint does not influence the response [28]. The acceleration of the center of gravity of the head and intracranial pressures

were compared with experimental data. The model configuration is shown in Figure 18. The measured impact force profile used to drive the model is shown in Figure 19.

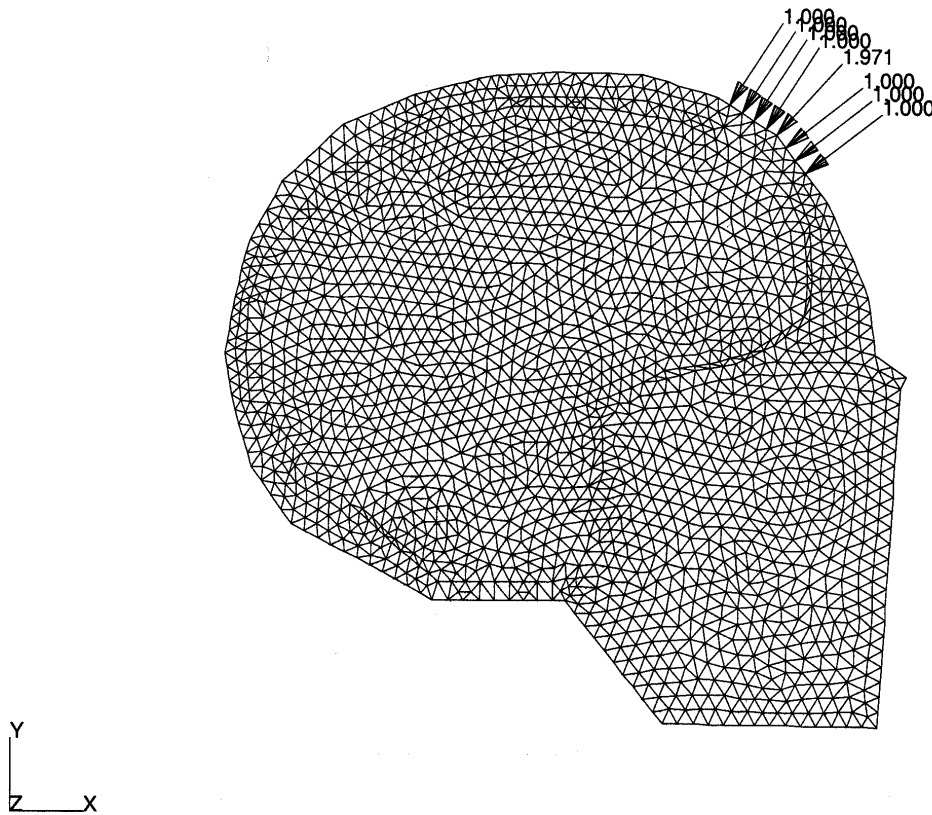


Figure 18. Frontal Impact Model Configuration.

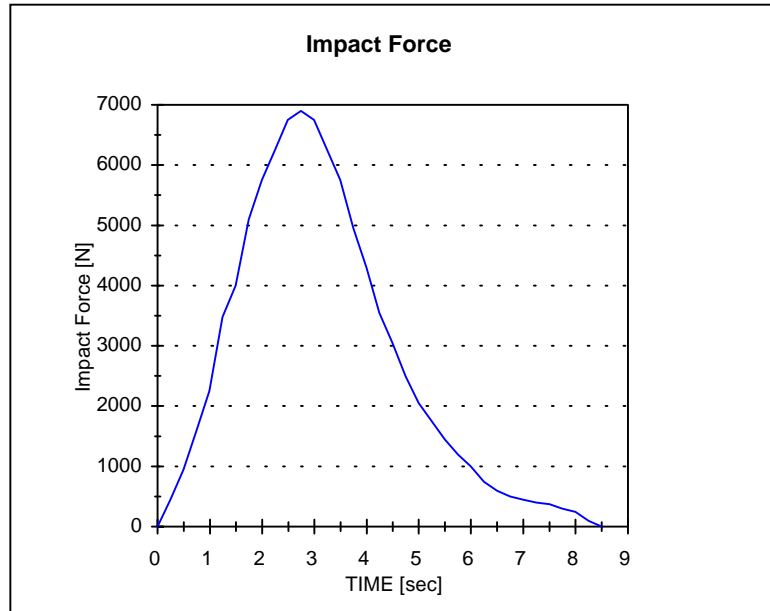


Figure 19. Impact Force

b. Results

Figure 20. shows the time history of acceleration of the center of gravity of the head. The model response correlates well with the experimental data in terms of overall curve shape and magnitude, although, a time delay is observed in the model response. This discrepancy may be due to the selection of linear elastic material properties for the brain. Several researchers have concluded that the response of the brain is sensitive to both Young's Modulus and Poisson Ratio [7,24,31,35]. Also, when a comparison of linear elastic and viscoelastic material properties was made using the same model, using viscoelastic material properties gave better results [7,32].

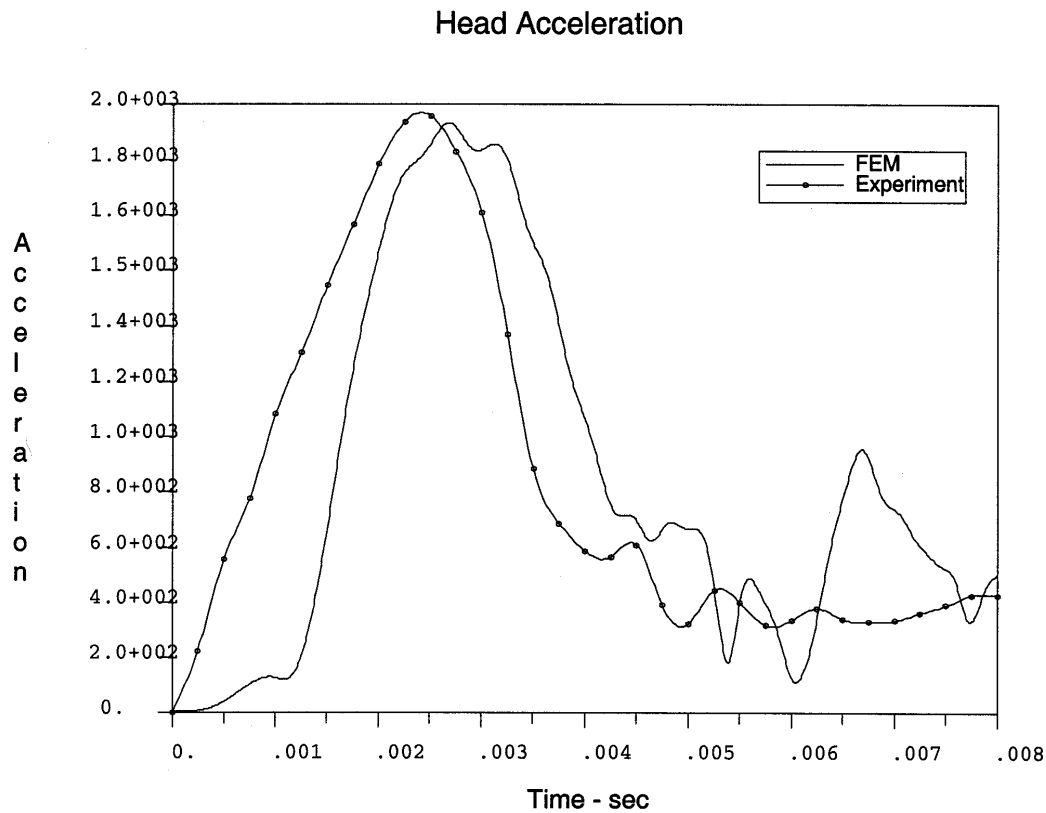


Figure 20. Head Acceleration

The post processor, PATRAN gives pressure measurements in terms of hydrostatic stress, where compression corresponds to a negative value and tension is given as a positive value. The experimental pressure data was replotted with this sign change (as hydrostatic stress) in order to make a direct comparison with the model response data. The hydrostatic stress comparisons will be referred to as "pressures" in the following discussion. Figure 21. shows a comparison of the pressure time history at the impact, or coup site. The correlation of the model

response and experimental data was excellent. The time lag seen in the acceleration response is not observed here since the pressure measurement was taken near the impact site.

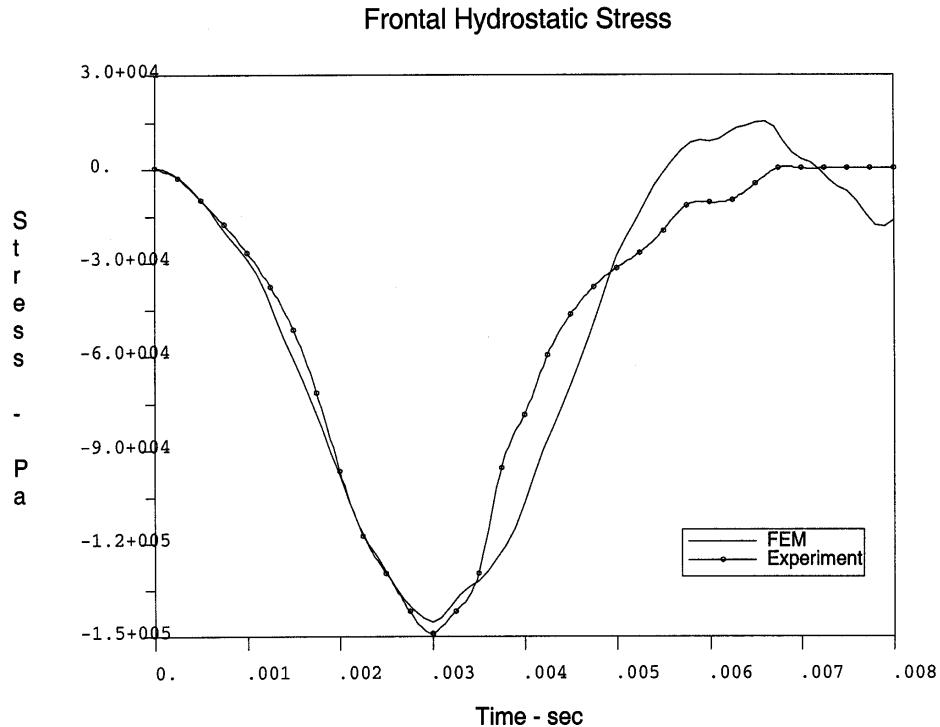


Figure 21. Frontal Hydrostatic Stress (Pressure)

The pressure time history at the contrecoup site, measured at the posterior fossa, is shown in Figure 22. The model agreed well with the experimental data in terms of curve shape but the magnitude of the contrecoup pressure was too high. This may be due to the model not sufficiently representing the pressure release mechanism offered by the foramen magnum at the base of the skull. Although the foramen magnum is modeled, brain tissue and fluid cannot move through it to the extent that it does in

reality. Adding a complete spinal cord and surrounding fluid to the model could possibly reduce the coup pressure.

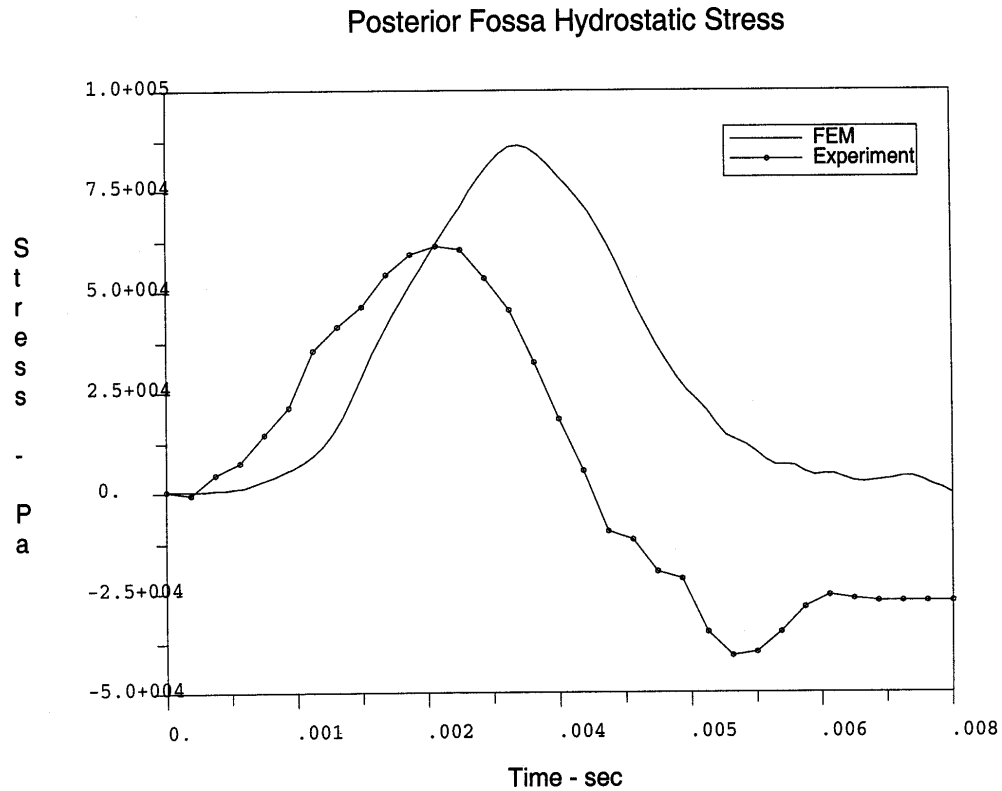


Figure 22. Posterior Fossa Hydrostatic Stress (Pressure)

In the experiments, pressure in the occipital region was measured in two locations laterally equidistant from the midline of the head in order to check for a symmetrical response. The two measurements are shown in Figure 23. as experiment 1 and experiment 2. Since the off center measurement was not possible in the 2D model the occipital pressure was approximated at the midline location. With this approximation in mind basic curve shape and magnitude were considered as comparison criteria. The general shape of the curve agreed well with

experimental data but the magnitude of the pressure was somewhat too high

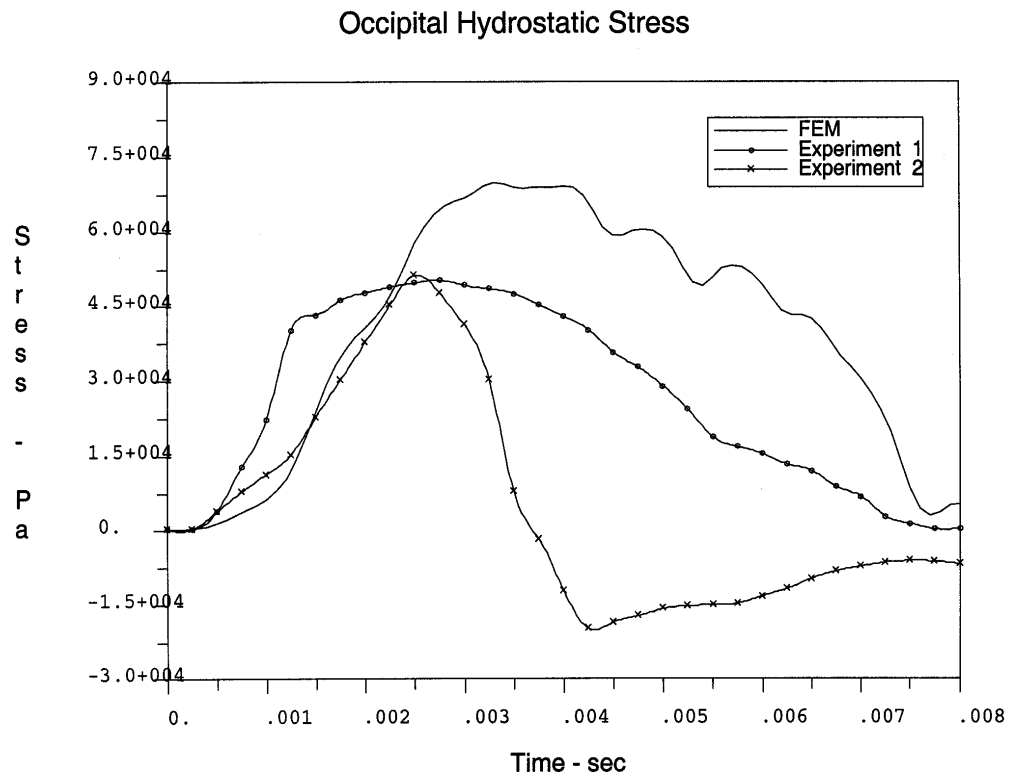


Figure 23. Occipital Hydrostatic Stress (Pressure)

Another approximate location was used to compare the Parietal pressure time history measurement as shown in Figure 24. The model response correlated well in terms of curve shape and magnitude but the model predicted a negative pressure (tensile stress) response after 5 ms that did not occur in the experiment.

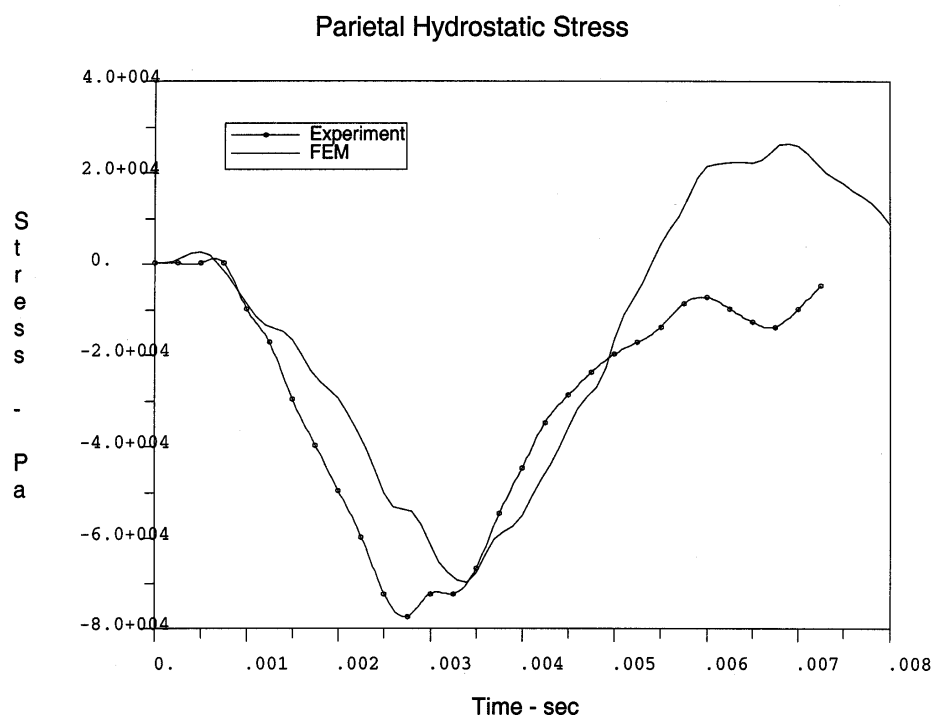


Figure 24. Parietal Hydrostatic Stress (Pressure)

Figure 25 shows the pressure distribution across the brain at 3 ms, which corresponds to the peak force. The pressure is linearly distributed across the brain with compression at the impact site and tension at the contrecoup location. This typical coup-contrecoup phenomenon agrees with experimental data as well as the response of finite element models of Ruan [28], Zhou [39] and Kang [14].

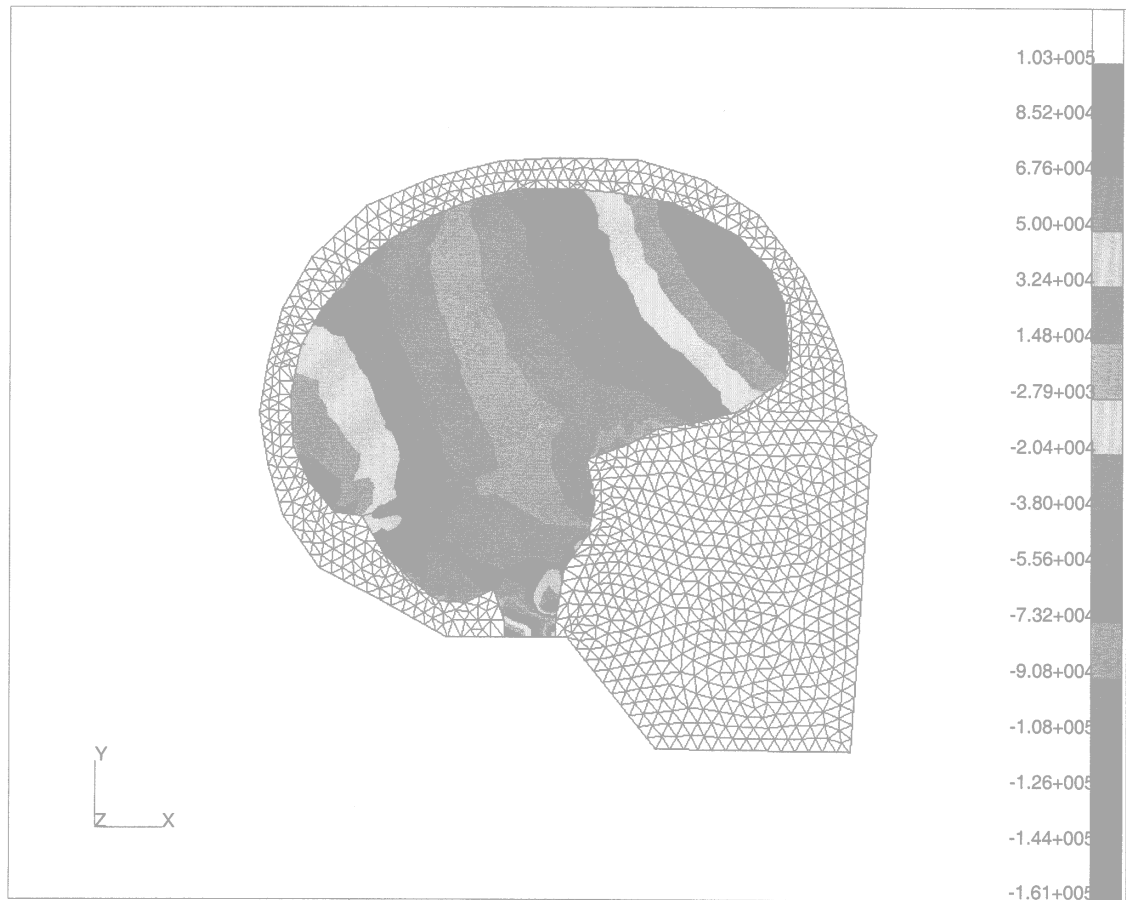


Figure 25. Hydrostatic Stress (Pressure) Contours at 3 ms

B. PARAMETRIC STUDY

The validated model was used to conduct a 2 part parametric study. First, the biodynamical response was examined under direct head impact to the frontal, occipital and crown regions of the head. Four impact force profiles of different peaks, rate of onset and pulse duration were applied directly to the model, simulating different conditions of loading that could result from direct impact. The three force profiles shown in Figure 26. and the force profile from the validation case (Figure 19) were used. Force profiles 805 and 410 have the same area under the

curve while force profiles 805 and 810 have the same peak force. Force profiles 810 and 410 have the same duration. All of the profiles have different rates of loading. These parameters were chosen in order to assess their respective influence on the response of the head. The head acceleration, intracranial pressures and maximum brain shear stress are measured and compared with the resulting Head Injury Criteria (HIC) values in order to evaluate the effectiveness of HIC in predicting injury.

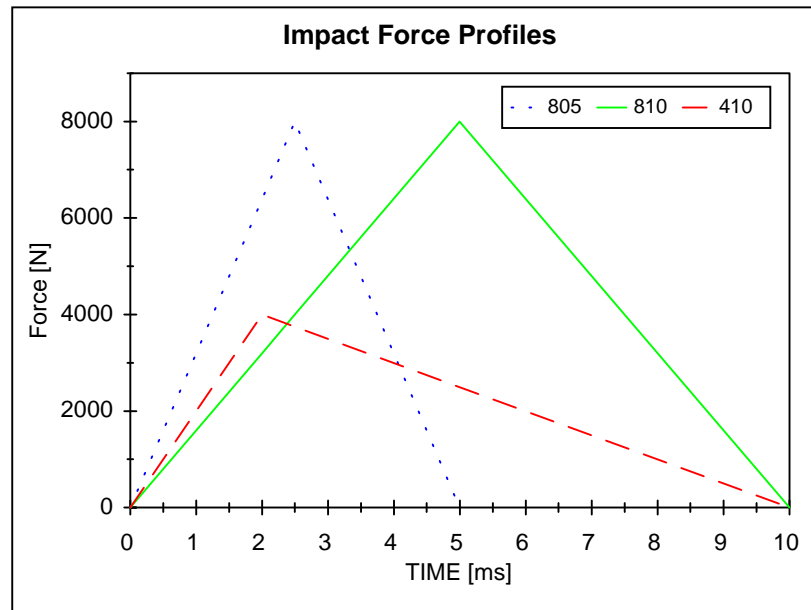


Figure 26. Force Profiles Used in Parametric Study.

For the second part of the parametric study, the effects of variations in impactor mass and initial velocity were examined. An Impactor was modeled as a 2D solid directly attached at the frontal, occipital and crown regions of the skull. Different values of mass and initial

velocity were applied to the impactor geometry as shown in Table 5. The values were selected such that the different values of mass and initial velocity resulted in the same value of momentum and kinetic energy for two of the cases respectively. This was done in order to assess the importance of these measures on the head response. The peak head acceleration, coup and contrecoup pressures from the simulations were recorded.

Case	Mass [kg]	Velocity [m/s]	Momentum (MV)	Kinetic Energy ($\frac{1}{2} MV^2$)
M ₁ V ₁	0.43	10	4.3	43
M ₂ V ₂	0.215	20	4.3	86
M ₂ V ₃	0.215	14.14	3.04	42.99
M ₁ V ₂	0.43	20	8.6	172

Table 5. Impactor Mass and Initial Velocity.

1. Effects of impact force characteristics

Figure 27. shows the effect of the different force profiles on head acceleration. Higher peak forces resulted in higher accelerations. But shorter impact resulted in higher acceleration than a longer duration impact of the same peak force. This indicates that loading rate and duration are important. No particular location of impact consistently corresponded to higher accelerations. Therefore it is concluded that acceleration of the head due to direct impact is a function of peak force, and to a lesser degree, loading rate and impact duration, and is independent of location of impact.

The magnitude of the coup and contrecoup pressures are shown for different impact locations in Figure 28. For each force profile the frontal impact coup pressure was the

lowest and the occipital impact coup pressure was the highest. The highest contrecoup pressure occurred with frontal impacts while the lowest occurred with crown impacts where some pressure release through the foramen magnum was possible. The higher peak force with shorter duration caused the highest coup and contrecoup pressures for all cases except occipital impact coup pressure where the higher peak force with longer duration caused the highest pressure. Since the higher peak force-shorter duration impact also corresponded to the highest acceleration it appears that peak acceleration may be an indicator of pressure magnitude.

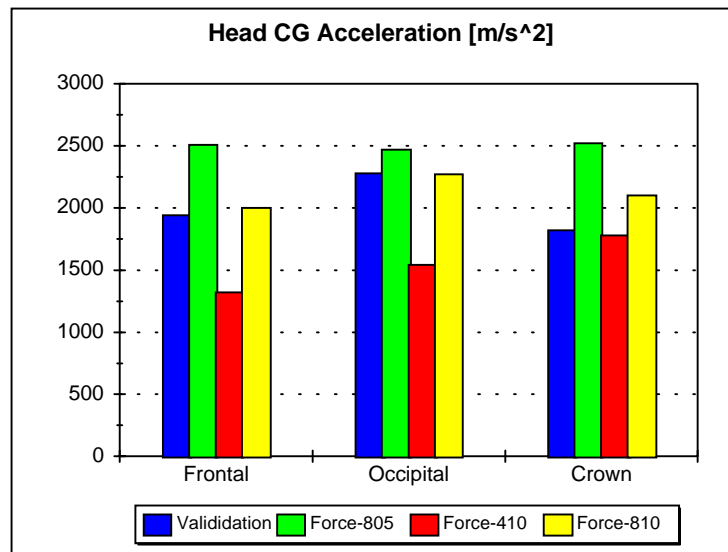


Figure 27. Head CG Acceleration by Location.

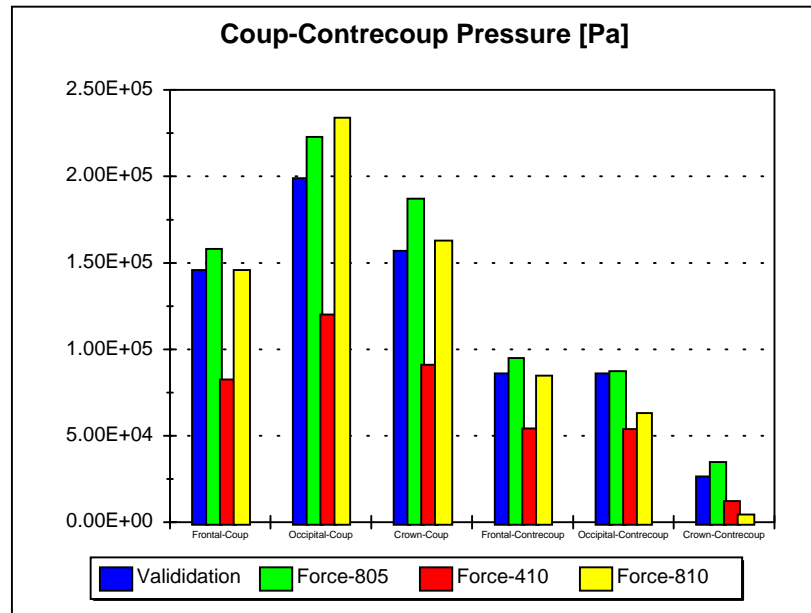


Figure 28. Pressure by Location.

Figure 29. is a plot of the coup and contrecoup pressures versus peak head acceleration for frontal impacts. From this graph it can be seen that pressure does in fact increase with peak acceleration but not at a linear rate. More data points would be needed to ascertain if any functional relationship in fact exists.

Figure 30. shows the pressure versus acceleration for occipital impacts. Again it can be seen that, in general, pressure increases with increasing peak acceleration but there is a jump in pressure where two data points have nearly the same acceleration. This indicates that there is a range of variability in pressure at a single acceleration value that may be due to another factor. In this case the data point with a higher pressure corresponded to the higher peak force-longer duration profile.

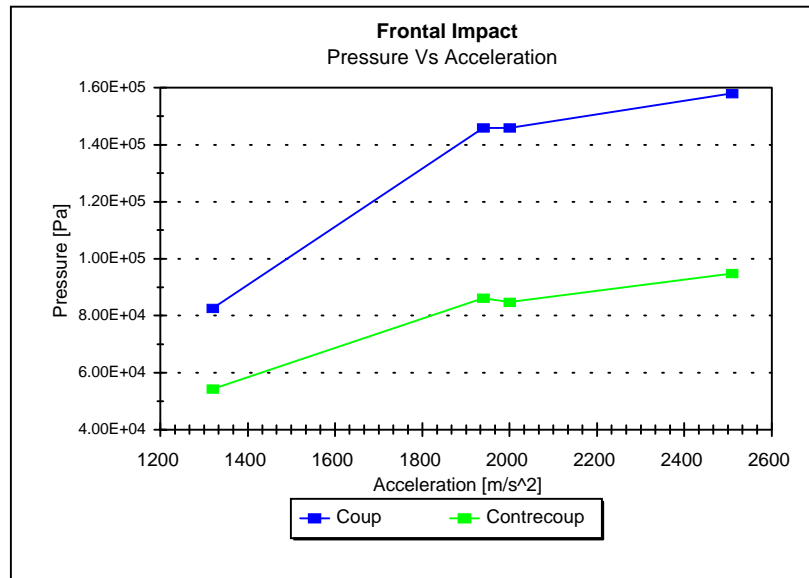


Figure 29. Pressure Versus Acceleration for Frontal Impact.

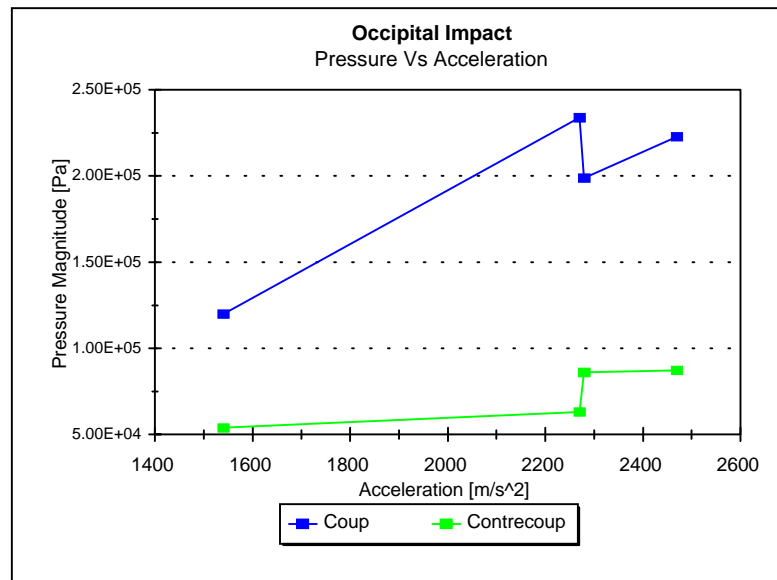


Figure 30. Pressure Versus Acceleration for Occipital Impact.

For crown impacts, the trend is also increasing pressure with increasing peak acceleration as shown in Figure 31. But this time the jump in pressure at nearly identical acceleration values is more severe for higher peak force-shorter duration impacts. It would appear that the influence of duration of impact depends on location but more data points would be needed to test this hypothesis.

HIC was calculated for each force profile run. Figure 32 shows how HIC varied with impact location. The highest HIC values for all loading conditions occurred with occipital impacts. This also corresponds to the highest coup pressures as seen previously in Figure 28. Therefore, based on HIC and coup pressure, occipital impacts will be the most severe for a given loading similar to the force profiles used in this study.

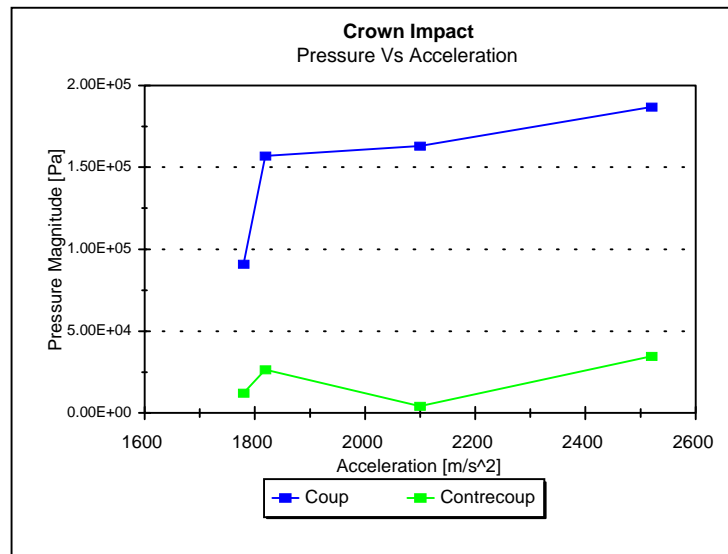


Figure 31. Pressure Versus Acceleration for Crown Impact.

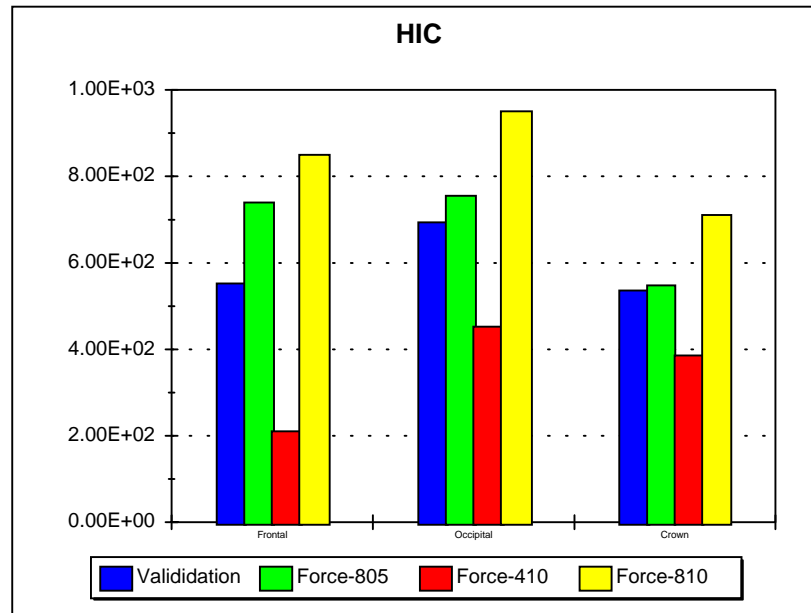


Figure 32. HIC by Location.

Figure 33. shows a comparison of the normalized coup pressure, contrecoup pressure, maximum brain shear stress, and HIC, versus peak head acceleration for frontal impacts. For all the cases, regardless of location of impact, the maximum brain shear stress occurred in the brain stem. It can be seen that HIC follows a similar trend as to brain shear stress and to a lesser extent coup and contrecoup pressures. This is especially true at higher accelerations where HIC and brain shear stress start to decrease with increased acceleration while coup and contrecoup pressures are still increasing. This indicates that HIC may only be an indicator of injury potential for a certain range of acceleration.

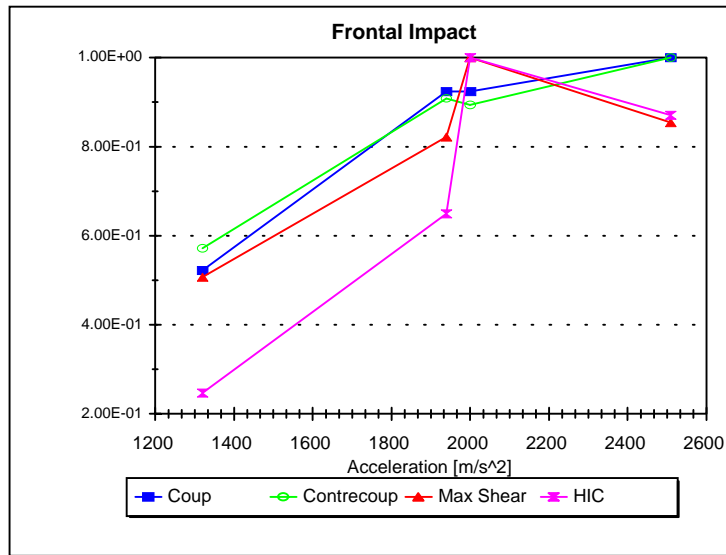


Figure 33. Normalized Parameters Versus Acceleration for Frontal Impact.

A similar trend is observed for occipital impacts in Figure 34. In this case HIC does not correlate with contrecoup pressure at the lower range of accelerations but does correlate much better at the higher level of acceleration. Again this shows that HIC is not a good predictor of all the injury causing parameters over the full range of accelerations.

For crown impacts, shown in Figure 34., it is clear that HIC does not correlate with the parameters at higher acceleration values but seems to be reasonable in the lower range.

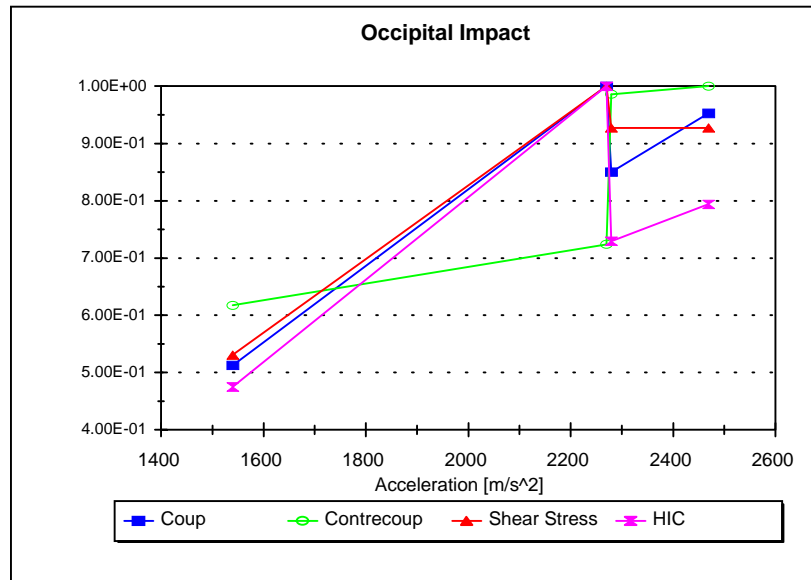


Figure 34. Normalized Parameters Versus Acceleration for Occipital Impact.

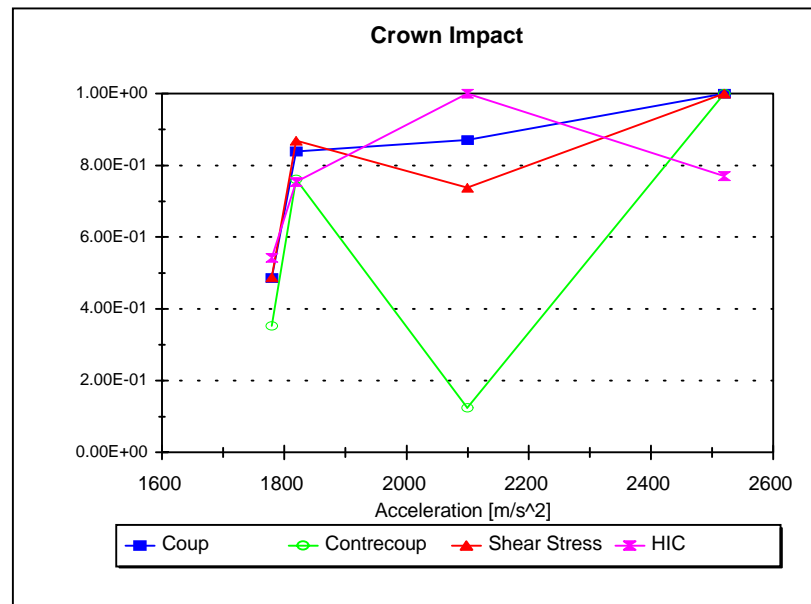


Figure 35. Normalized Parameters Versus Acceleration for Crown Impact.

2. Effects of impactor characteristics

Figure 36. indicates the effect of changing mass and initial velocity on head acceleration. The effect of doubling the velocity while keeping mass constant can be seen going from case M1-V1 to M1-V2. The effect of doubling the mass while keeping velocity the same can be seen in going from case M2-V2 to M1-V2. Clearly, velocity has more of an effect than mass. This indicates that the peak head acceleration is more closely related to kinetic energy rather than momentum since momentum is proportion to velocity and kinetic energy is proportional to the square of the velocity. Contrary to the force profile results in Figure 27, the acceleration depends on impact location. The accelerations were highest for frontal impacts and lowest for occipital impacts. It is unclear exactly what is influencing this result but it may be due to the overall higher accelerations of the mass-velocity runs. It is possible that at high values of acceleration the functional relationship of the head response changes.

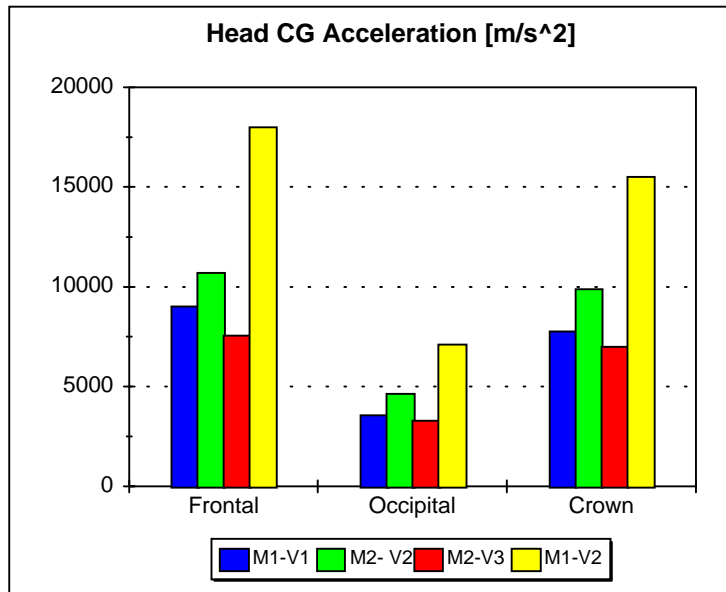


Figure 36. Head CG Acceleration by Location.

Figure 37. shows the resulting pressure from the different mass-velocity combinations. The highest coup pressure occurred with frontal impacts while the lowest was seen with crown impacts. The highest contrecoup pressure occurred with occipital impacts while the lowest occurred with frontal impacts. The higher mass, higher velocity combination (M1-V2), resulted in the highest pressures while the lowest mass with the middle value of velocity resulted in the lowest pressures. These results do not agree with the force profile results shown in figure 28. There appears to be a shift in dominant pressure, whether coup or contrecoup, for occipital and crown impacts where for higher accelerations the contrecoup mechanism has higher pressure magnitudes than the coup mechanism. This can be seen more clearly by comparing the plots of pressure versus acceleration at the different impact locations for

the mass-velocity runs (Figures 38-40), with those of the force profile runs.

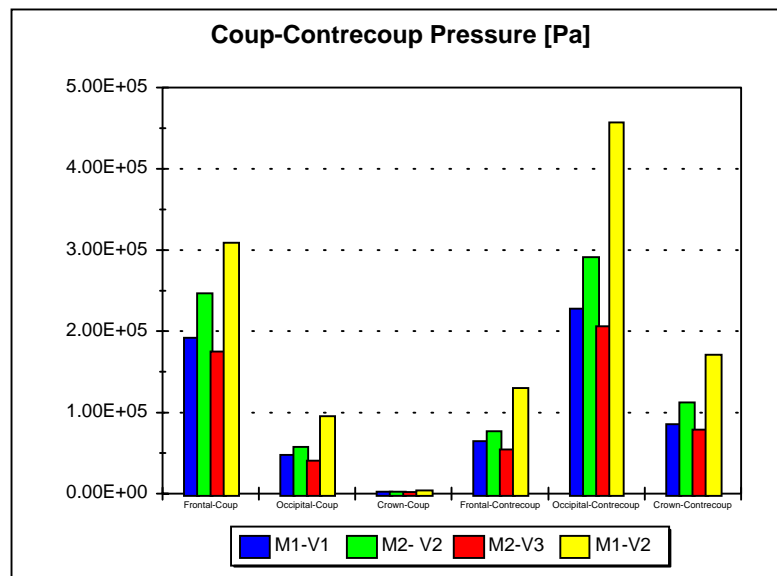


Figure 37. Pressure by Location.

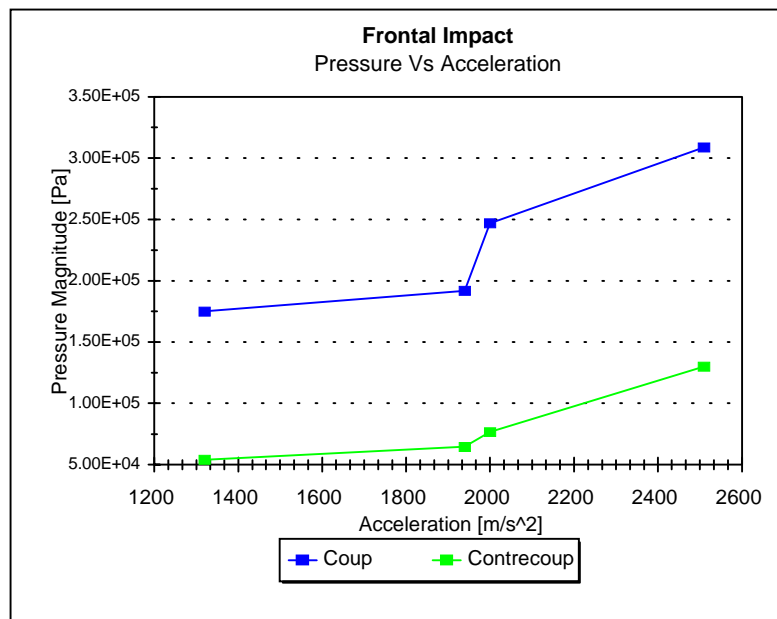


Figure 38. Pressure Versus Acceleration for Frontal Impact.

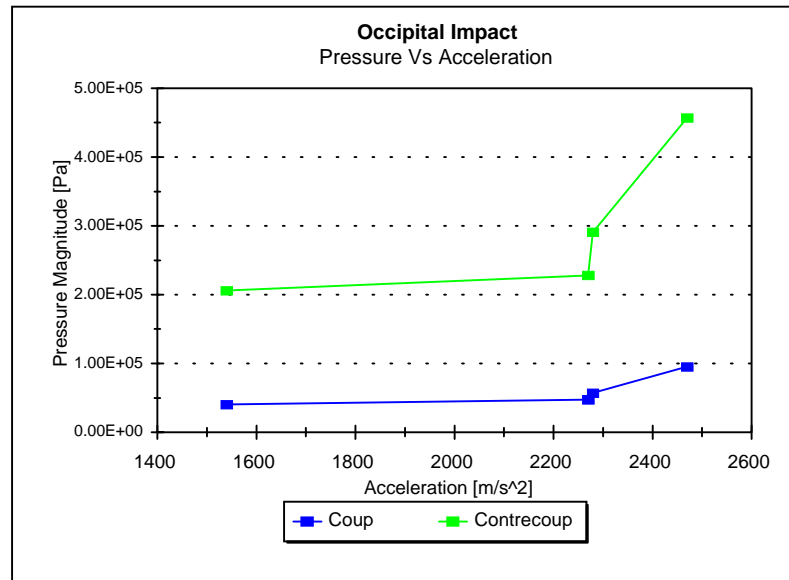


Figure 39. Pressure Versus Acceleration for Occipital Impact.

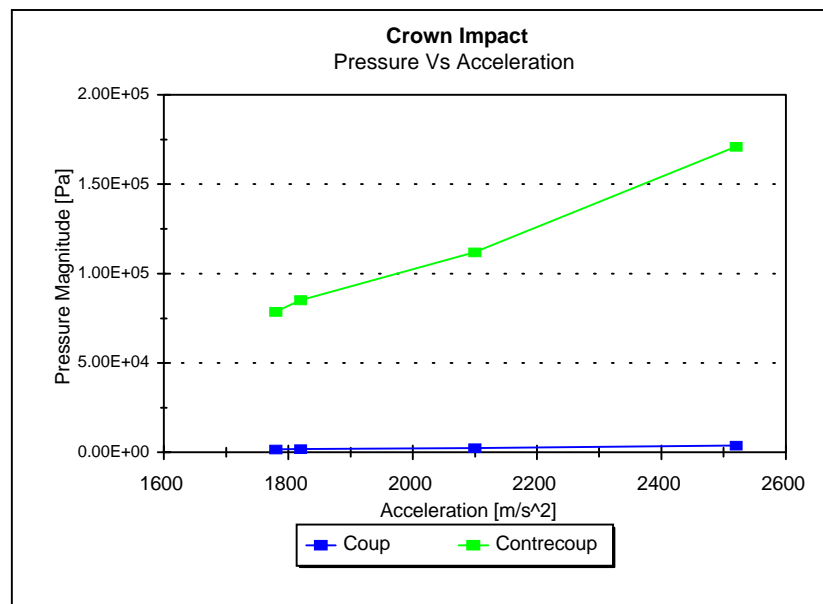


Figure 40. Pressure Versus Acceleration for Crown Impact.

Figure 41 is a plot of the peak head acceleration versus the impactor momentum for frontal, occipital and crown impacts. In general acceleration appears to increase with increasing momentum. However, at the two data points having the same momentum, the one with higher acceleration corresponded to the case with lower mass and higher velocity. The same relationship holds for the plot of pressure versus momentum as shown in Figure 42. Where, for constant momentum, the higher pressure corresponds to the case with lower mass and higher velocity. This indicates that for a given momentum, a relative increase in velocity has more injurious effects than an increase in mass.

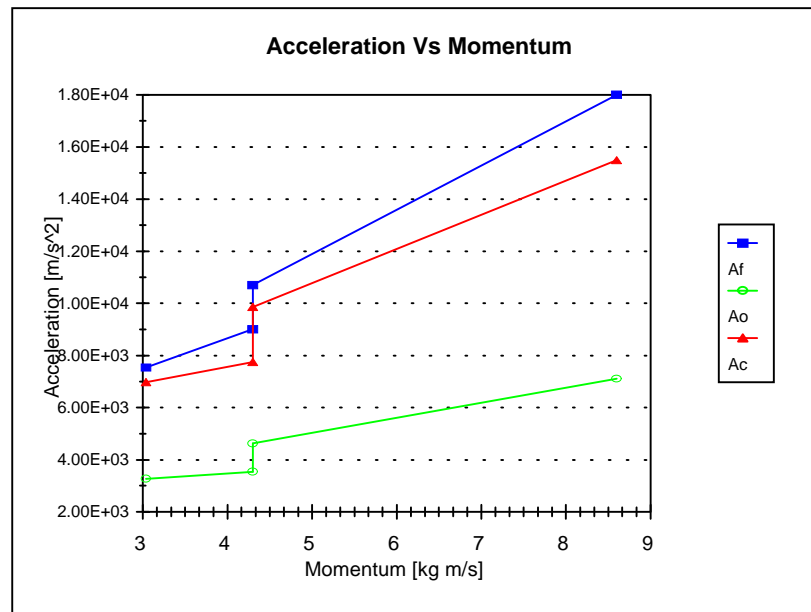


Figure 41. Acceleration Versus Momentum for Frontal, Occipital and Crown Impacts.

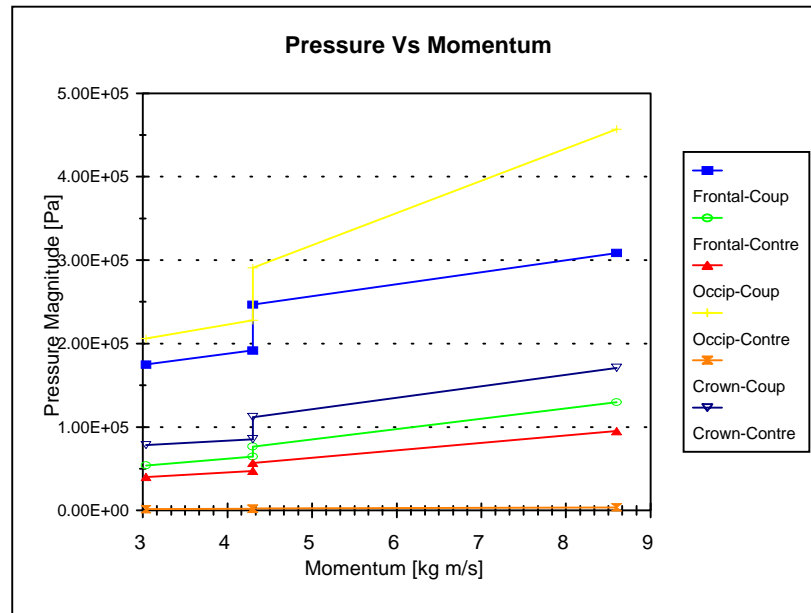


Figure 42. Pressure Versus Momentum for Frontal, Occipital and Crown Impacts.

The peak head acceleration versus the impactor kinetic energy is plotted in Figure 43. Overall, the acceleration increases with increasing kinetic energy. The peak acceleration seems to have a more linear relationship with kinetic energy of the impactor than it did with momentum. But there is still a difference in acceleration for the two data points with the same kinetic energy. This time the higher acceleration corresponds to the case with higher mass and lower velocity. The same trend is also seen in Figure 44. with the pressure plotted against kinetic energy of the impactor. Basically, the pressure follows an increase in peak acceleration in both the constant momentum and constant kinetic energy cases.

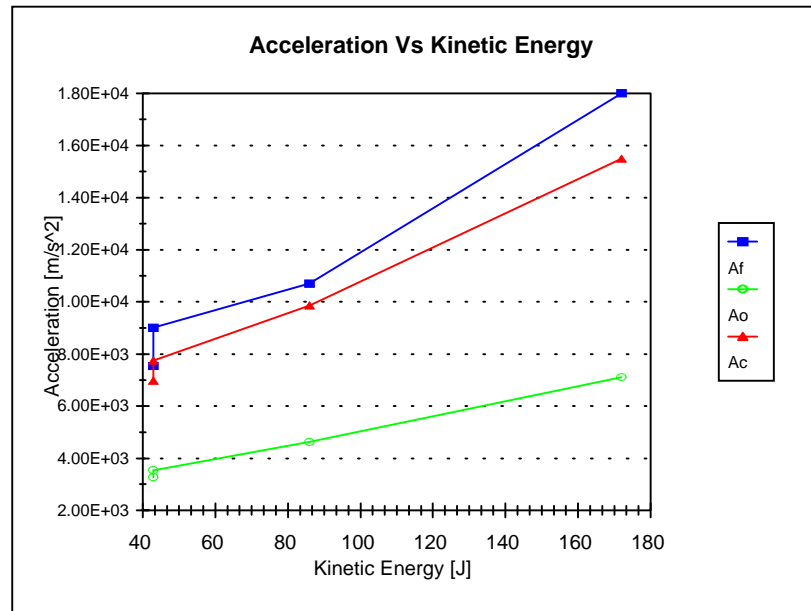


Figure 43. Acceleration Versus Kinetic Energy for Frontal, Occipital and Crown Impacts.

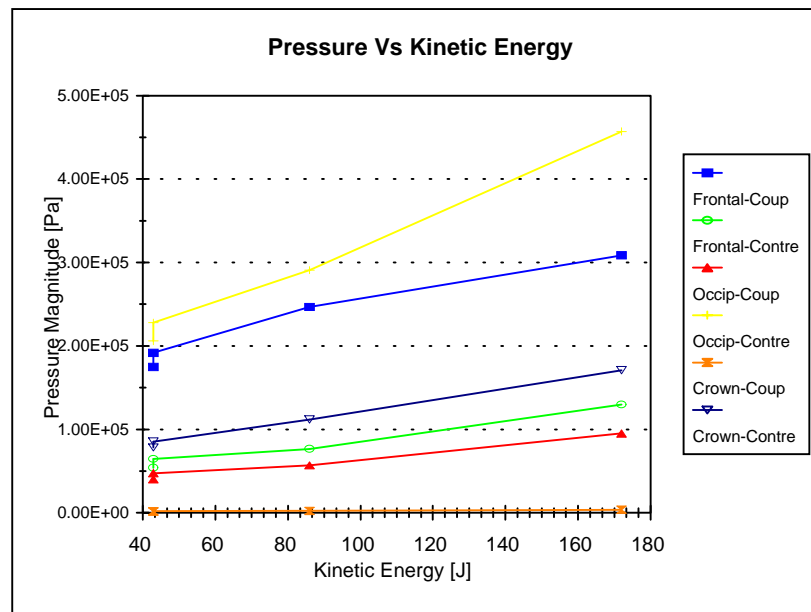


Figure 44. Pressure Versus Kinetic Energy for Frontal, Occipital and Crown Impacts.

VI. CONCLUSIONS AND RECOMMENDATIONS

A. CONCLUSIONS

The objective of this study was to develop a finite element model of the human head and neck such that the model adequately predicts the biodynamical response to direct head impact and inertial loading. The model was used to investigate the biomechanics of head injury and associated injury mechanisms, and then to evaluate the ability of HIC to predict injury. The dynamic response of the head-neck model was validated by comparison with the results of human volunteer sled acceleration experiments. Validation of the head model was accomplished by comparing the model's response with measured cadaveric impact test data. Once the model was validated, a parametric study was conducted to determine the effects of different impact force profiles, location of impact and impactor characteristics.

The results of the parametric study demonstrate that HIC, which is based on resultant translational acceleration of the center of gravity of the head, does not relate to the various mechanisms of brain injury and is therefore insufficient in predicting brain injury.

From the results of the force profile parametric study the following conclusions can be made:

Impact location is an important parameter. The magnitude of all the measured parameters except for acceleration, varied with location.

Max brain shear stress always occurs in the brain stem and maybe responsible for brain stem laceration observed clinically.

HIC was not consistently proportional to the various injury causing parameters over the full range of acceleration values. Therefore, a single parameter injury tolerance criterion is insufficient. Tolerance criteria should be based on the cumulative effect of the thresholds for each of the injury causing mechanisms

From the impactor mass and velocity study it was found that velocity had more of an effect on the response than mass. Although for a constant impactor kinetic energy, mass was an important factor.

For both parametric studies pressure seemed to be related to the peak acceleration. For the mass-velocity studies, the modeling simulated a short impact with a very fast rise time and relatively higher accelerations than the force profile study. This made direct comparison between the two studies difficult. It seemed that for the higher accelerations that occurred with the mass-velocity study the contrecoup pressures were dominant for occipital and crown impacts.

This study has shown that a validated finite element model can be a valuable tool in investigating head injury mechanisms and formulating injury tolerance criteria related to specific mechanisms. Improved protection against head injury can be realized through a better understanding of the biomechanics of injury and disability gained through finite element modeling.

B. RECOMMENDATIONS

It is recommended that follow on research include:

Investigate model response to different translational and rotational acceleration inputs and evaluate the effectiveness of HIC in predicting head injury. HIC only accounts for translational acceleration but rotational acceleration may be an additional important factor in brain injury that HIC cannot predict.

Add muscle and ligament representation to the neck model and investigate more effective method for modeling facet joints. Upon validation of revised neck model, conduct a whiplash study using the head-neck model. This study looked at direct head impacts. Additional loading conditions should be examined, such as inertial loading where impact does not occur.

Extend the model to 3D. A three dimensional model would allow the modeling of additional important structures in the brain as well as achieving a more realistic head model. A 3D model could be used to study a variety of loading conditions such as side and multiple location impacts.

THIS PAGE INTENTIONALLY LEFT BLANK

LIST OF REFERENCES

1. Al-Bsharat, A. S., Hardy, W. N., Yang, K. H., Khalil, T. B., Tashman, S., King, A. I., "Brain/Skull Relative Displacement Magnitude Due to Blunt Impact: New Experimental Data and Model," Proceedings of the 43rd Stapp Car Crash Conference, 1999 (SAE 99SC22)
2. Alcamo, I. E., *Anatomy and Physiology the Easy Way*, Barron's New York, 1996.
3. Ashton-Miller, J. A., Shultz, A. B., 1997, "Biomechanics of the Human Spine" in: *Basic Orthopaedic Biomechanics: Second Edition*, Mow, V. C., Hayes, W. C., eds. Lipincott-Raven New York, pp 353-394.
4. Bandak, F. A., Eppinger, R. H., "A 3-Dimensional Finite Element Analysis of the Human Brain Under Combined Rotational and Translational Accelerations," Proceedings of the 38th Stapp Car Crash Conference, pp 145-163, 1994 (SAE 942215)
5. Bertholon, N., Robin, S., Skalli, W., Le Coz, J. Y., Lavaste, F., "Dynamic Model of the Human Head - Neck Complex,"
<http://www.utc.fr/esb/esb98/abs_htm/337.html>
6. Bo, W. J., Meschan, I., Kruegar, W. A., *Basic Atlas of Cross-Sectional Anatomy*, W. B. Saunders Company, 1980.
7. Claessens, M., Sauren, F., Wismans, J., "Modeling the Human Head Under Impact Conditions: A Parametric Study," Proceedings of the 41st Stapp Car Crash Conference, pp 315-328, 1997 (SAE 973338)
8. DiMasi, F. P., Bandak, F. A., Eppinger, R. H., "Computational Analysis of Head Impact Response Under Car Crash Loadings," Proceedings of the 39th Stapp Car Crash Conference, pp 425-438, 1995 (SAE 952718)
9. Douglass, J. M., Nahum, A. M., Roberts, S. B., "Applications of Experimental Head Injury Research," Proceedings of the 13th Stapp Car Crash Conference, pp 317-337, 1968 (SAE 680786)
10. Ewing, C. L., and Thomas, D. J., 1972 "Human Head and Neck Response to Impact Acceleration," NAMRL monograph 21, Naval Aerospace Medical Research Laboratory, Pensacola, FL.
11. Family Caregiver Alliance, *Fact Sheet: Selected Head Injury Statistics*, San Francisco, CA.
<http://www.caregiver.org/factsheets/head_statsC.html>
12. Fan, W. R. S., "Internal Head Injury Assessment," Proceedings of the 15th Stapp Car Crash Conference, pp 645-665, 1971 (SAE 710870)
13. Gray, H., *Anatomy: Descriptive and Surgical*, 15th ed, Barnes and Noble Books, 1995.

14. Kang, H., Willinger, R., Diaw, B. M., Chinn, B., "Validation of a 3D Anatomic Human Head Model and Replication of Head Impact in Motorcycle Accident by Finite Element Modeling," Proceedings of the 41st Stapp Car Crash Conference, pp 329-338, 1997 (SAE 973339)
15. Khalil, T. B., Viano, D. C., "Critical Issues in Finite Element Modeling of Head Impact," Proceedings of the 26th Stapp Car Crash Conference, pp 87-102, 1982 (SAE 821150)
16. King, Q. M., 1998, "Investigation of Biomechanical Response Due to Fragment Impact on Ballistic Protective Helmet," Master's Thesis, Naval Postgraduate School, Monterey, CA.
17. Krabbel, G., Muller, R., "Development of a Finite Element Model of the Head Using the Visible Human Data," The Visible Human Project Conference, 1996, National Institute of Health, Bethesda, Maryland (USA), <http://www.kfz.tu-berlin.de/broschuere/projekte/kopfschutz/vhp_tu.html>
18. Lee, K., 1998, "Biomechanical Response of the Human Body Inside a Military Vehicle Exposed to Mine Explosion," Master's Thesis, Naval Postgraduate School, Monterey, CA.
19. Lee M. C., Melvin, J. W., Ueno, K., "Finite Element Analysis of Traumatic Subdural Hematoma," Proceedings of the 31st Stapp Car Crash Conference, pp 67-77, 1987 (SAE 872201)
20. McElhaney, J. H., Myers, B. S., 1993, "Biomechanical Aspects of Cervical Trauma" in: *Accidental Injury: Biomechanics and Prevention*, Nahum, A. M., Melvin, J., eds. Springer-Verlag New York, pp 311-361.
21. Mehta, B. V., Mulabagula, R., Patel, J. V., "Finite Element Analysis of the Human Skull Considering Brain and Bone Material Properties," <<http://www.ent.ohiou.edu/~mehta/skulluk.html>>
22. Melvin, J. W., Lighthall, J. W., Ueno, K., 1993, "Brain Injury Biomechanics" in: *Accidental Injury: Biomechanics and Prevention*, Nahum, A. M., Melvin, J., eds. Springer-Verlag New York, pp 268-291.
23. Miller, R. T., Margulies, S. S., Leoni, M., Nonaka, M., Chen, X., Smith, D. H., Meaney, D. F., "Computational Analysis of Head Impact Response Under Car Crash Loadings," Proceedings of the 42nd Stapp Car Crash Conference, pp 1-13, 1998 (SAE 983154)
24. Nahum A. M., Smith, R., Ward, C. C., "Intracranial Pressure Dynamics During Head Impact," Proceedings of the 21st Stapp Car Crash Conference, pp 339-366, 1977 (SAE 770922)
25. National Institute of Neurological Disorders and Stroke, National Institute of Health, 2000, September *Interagency Head Injury Task Force Report*, Bethesda, MD. <<http://www.biact.org/tbistats.html>>
26. Newman, J. A., "Head injury Criteria in Automotive Crash Testing," Proceedings of the 24th Stapp Car Crash Conference, pp 704-747, 1980 (SAE 801317)

27. Olson, T. R., *A.D.A.M. Student Atlas of Anatomy*, Williams & Wilkins Baltimore, MD 1996.
28. Ruan, J. S., Khalil, T. B., King, A. I., "Finite Element Modeling of Direct Head Impact," Proceedings of the 37th Stapp Car Crash Conference, pp 69-81, 1993 (SAE 933114)
29. Stalnaker, R. L., Burke, W. V., Hines, M. H., "The Translational Energy Criteria: A Validation Study for Non-Fracture Head Impacts," Proceedings of the 41st Stapp Car Crash Conference, pp 301-314, 1997 (SAE 973337)
30. Toga, Arthur W., 1999, "Human Brain," CDROM Microsoft Encarta Encyclopedia 99.
31. Trosseille, X., Tarriere, C., Lavaste, F., Guillon, F. Domont, A., "Development of a F. E. M. of the Human Head According to a Specific Test Protocol," Proceedings of the 36th Stapp Car Crash Conference, pp 235-253, 1992 (SAE 922527)
32. Turquier, F., Kang, H., Trosseille, X., Willinger, R., Lavaste, F., Tarriere, C., Domont, A., "Validation Study of a 3D Finite Element Head Model Against Experimental Data," Proceedings of the 40th Stapp Car Crash Conference, pp 283-294, 1996 (SAE 962431)
33. Viano, D. C., "Biomechanics of Head Injury - Toward a Theory Linking Head Dynamic Motion, Brain Tissue Deformation and Neural Trauma," Proceedings of the 32nd Stapp Car Crash Conference, pp 1-20, 1988 (SAE 881708)
34. Ward, C. C., Thompson, R. B., "The Development of a Detailed Finite Element Brain Model," Proceedings of the 19th Stapp Car Crash Conference, pp 641-674, 1975 (SAE 751163)
35. Ward, C. C., Chan, M., Nahum, A., "Intracranial Pressure - A Brain Injury Criterion," Proceedings of the 24th Stapp Car Crash Conference, pp 163-185, 1980 (SAE 801304)
36. Ward, C. C., "Finite Element Models of the Head and Their Use in Brain Injury Research," Proceedings of the 26th Stapp Car Crash Conference, pp 71-85, 1982 (SAE 821154)
37. White, A. A., and Panjabi, M. M., *Clinical Biomechanics of the Spine*, Lippincott-Raven New York, 1990.
38. Williams, J. L. and Belytscho, T. B., 1983, "A Three Dimensional Model of the Human Cervical Spine for Impact Simulation," *Journal of Biomechanics*, Vol. 105, pp. 321-331.
39. Zhou, C., Khalil, T. B., King, A. I., "A New Model Comparing Impact Response of the Homogeneous and Inhomogeneous Human Brain," Proceedings of the 39th Stapp Car Crash Conference, pp 121-137, 1995 (SAE 952714)

THIS PAGE INTENTIONALLY LEFT BLANK

INITIAL DISTRIBUTION LIST

1. Defense Technical Information Center 2
Ft. Belvoir, VA 22060-6218
2. Dudley Knox Library 2
Naval Postgraduate School
Monterey, CA
3. Professor Terry R. McNelley 1
Department of Mechanical Engineering
Naval Postgraduate School
Monterey, CA
tmcnelley@nps.navy.mil
4. Professor Young W. Kwon ME/Kw 2
Department of Mechanical Engineering
Naval Postgraduate School
Monterey, CA
ywkwon@nps.navy.mil
5. Naval Engineering Curricular Office (code 34) 1
Naval Postgraduate School
Monterey, CA
tmccoy@nps.navy.mil
6. Danielle N. George, LT, USN 2
madaboutu2@hotmail.com